

INCONEL 625 AND STAINLESS STEEL 316L DUAL WIRE ARC ADDITIVE MANUFACTURING OF FUNCTIONALLY GRADED MATERIALS

M.Tech. Thesis

By
ANSHUMAN DADHICH
(2002103002)



**DEPARTMENT OF MECHANICAL ENGINEERING
INDIAN INSTITUTE OF TECHNOLOGY INDORE**

MAY 2022

**INCONEL 625 AND STAINLESS STEEL 316L
DUAL WIRE ARC ADDITIVE
MANUFACTURING OF FUNCTIONALLY
GRADED MATERIALS**

A THESIS

*Submitted in partial fulfillment of the
requirements for the award of the degree
of
Master of Technology*

by
**ANSHUMAN DADHICH
(2002103002)**



**DEPARTMENT OF MECHANICAL ENGINEERING
INDIAN INSTITUTE OF TECHNOLOGY
INDORE**

MAY 2022



INDIAN INSTITUTE OF TECHNOLOGY INDORE

CANDIDATE'S DECLARATION

I hereby certify that the work which is being presented in the thesis entitled **Inconel 625 and Stainless Steel 316L Dual Wire Arc Additive Manufacturing of Functionally Graded Materials** in the partial fulfillment of the requirements for the award of the degree of **MASTER OF TECHNOLOGY** and submitted in the **DEPARTMENT OF MECHANICAL ENGINEERING, Indian Institute of Technology Indore**, is an authentic record of my own work carried out during the time period from August 2020 to May 2022 under the supervision of **Dr. Yuvraj Kumar Madhukar**, Assistant Professor, Department of Mechanical Engineering, Indian Institute of Technology, Indore.

The matter presented in this thesis has not been submitted by me for the award of any other degree of this or any other institute.

Anshuman
01/06/2022
Anshuman Dadhich
(2002103002)

This is to certify that the above statement made by the candidate is correct to the best of our knowledge.

01/06/22

(Dr. Yuvraj Kumar Madhukar)

Mr. Anshuman Dadhich has successfully given his M.Tech. Oral Examination held on **May 23, 2022**.

01/06/22

Signature(s) of Supervisor(s) of M.Tech. thesis

Date:

Signature of PSPC Member #1

Dr. Hemant Borker

Date:

Gyish
Convener, DPGC

Date: 01/06/22

Ashish
01/06/2022

Signature of PSPC Member #2

Dr. Ashish Rajak

Date:

ACKNOWLEDGEMENT

My deep gratitude goes first to my supervisor, **Dr. Yuvraj Kumar Madhukar**, who expertly guided me throughout my two years of Master of Technology. I was fortunate to have advisors who offered me the constant motivation and productive support that preceded this work to attain this form. I would also like to thank my PSPC members, Dr. Hemant Borkar and Dr. Ashish Rajak for their continuous inputs for the advancement of this project.

A very special thanks to Mr. Anas Ullah Khan (Ph.D. scholar), for their moral support and supportive environment for the completion of the project. Thanks also goes to Mr. Satyaprakash Mahalik, Mr. Abhinav Katiyar, and my other batch-mates for their moral support throughout this journey. I am also thankful to Mr. Krishnapal Tomar, Lab manager, Laser Material Processing, IIT Indore.

I cannot end my words without expressing my heartfelt thanks and admiration for my dear parents' blessings and efforts to maintain my morale throughout my project. I would like to offer my heartfelt gratitude to everyone who has assisted me in any way, whether directly or indirectly, during this project.

With Regards,

Anshuman Dadhich

Dedicated to
My beloved mother Mrs. Suman
Dadhich and sisters
for their unwavering support
throughout the journey

ABSTRACT

Wire Arc Additive Manufacturing (WAAM) is a layer-by-layer manufacturing technology that has evolved into a potential solution for manufacturing large-scale metallic components with low and moderate structural complexity. This dissertation aims to narrowing the research to fabricate the Functionally Graded Materials (FGMs) of varying combinations of Stainless steel (SS316L) and Nickel-based (IN625) superalloy using WAAM. For the purpose, the Gas Tungsten Arc Welding (GTAW) was used as heat source, and the SS316L and IN625 wires were feed into the stabilized arc of GTAW. The wires were fed using the cold wire feeder and deposited layer by layer on the steel substrate. Functionally graded materials of SS316L and IN625 have an application in nuclear power plants, oil and gas industries (like marine risers), automotive industries, and where high-temperature strength and corrosion-resistant material are required. The process parameters were optimised to obtain the possible combination of weight percentage for both the materials. Sandwich and incremental gradient structure of various patterns were successfully fabricated. The deposited parts were observed to be free from defects such as microcracks and voids as confirmed by microstructure analysis. EDS scan and micro-indentation hardness were also analysed to investigated the gradient variation and mechanical properties. EDS line scan for the 10% incremental gradient samples showed the stair change, whereas the sandwich gradient wall shows alternate crest for the key element Ni and Fe.

Keywords: Wire Arc Additive Manufacturing, Stainless Steel, Nickel-based superalloy, Gas tungsten arc welding.

TABLE OF CONTENT

ABSTRACT	ix
TABLE OF CONTENT	xi
LIST OF FIGURES	xv
LIST OF TABLES	xix
ACRONYMS	xxi
Chapter 1	
Introduction	1
1.1. Overview	1
1.2. Functionally Graded Materials	1
1.3. Manufacturing Methods of FGMs	3
1.3.1. Conventional Techniques	4
1.3.2. Additive Manufacturing (AM)	6
1.4. Wire Arc Additive Manufacturing (WAAM)	12
Chapter 2	
Literature Review and Objective	15
2.1. Overview	15
2.2. Literature Review	15
2.3. Objectives of the Present Research Work	23
Chapter 3	
Experimental Setup and Parameter Optimisation	25
3.1. Overview	25
3.2. Experimental Setup	25
3.3. Optimisation of process parameters	28
Chapter 4	
Design and Research Methodology	31
4.1. Overview	31
4.2. Incremental Gradient Structure	31
4.3. Sandwich Gradient Structure	35
4.4. Research Methodology and Sample Preparation	38
Chapter 5	
Results and Discussion	41

5.1.	Overview	41
5.2.	Incremental Gradient Structure	41
5.3.	Sandwich Gradient Structure	47
Chapter 6		
	Conclusions and Future Scope	55
6.1	Overview	55
6.2	Conclusion	55
6.3	Future scope	57
	REFERENCES	59

LIST OF FIGURES

Figure 1.1 Applications of Functionally Graded Materials [4]	3
Figure 1.2 Schematics of different types of FGM [5]	4
Figure 1.3 A schematic representation of the material jetting process. [26].....	10
Figure 1.4 WAAM-TIG setup with dual wire feeding nozzles.....	13
Figure 2.1 Crack at 90%SS316L-10%IN625 in a non-preheated sample.	16
Figure 2.2 A FEM model of gradient alloy automotive valve stem [34]	19
Figure 2.3 Microhardness variation of FGM from bottom of the SS321 to the top of IN625.....	20
Figure 2.4 A schematic of FGM (SS316L-IN625).....	21
Figure 2.5 Hardness (Vickers) measurement of FGMs	22
Figure 3.1 Pictorial Representation of Dual wire fixture setup.....	25
Figure 3.2 Migatron TIG (350 AC/DC) power source	26
Figure 3.3 An experimental setup of WAAM-TIG	27
Figure 3.4 Process parameter optimisation for maximum wfs.....	28
Figure 3.5 Optimisation for minimum wfs	29
Figure 4.1 A schematic of the Incremental gradient structure of FGM31	
Figure 4.2 Front feeding of the wires during deposition	33
Figure 4.3 Alignment of the wires with the electrode	33
Figure 4.4 Stereoscopic view of the interface of AISI 1020 and SS316L	34
Figure 4.5 Incremental Gradient Structure wfs 4.0 m/min FGM of SS316L and IN625	34
Figure 4.6 Incremental Gradient Structure wfs 3.0 m/min FGM of SS316L and IN625	35
Figure 4.7 Schematic of AABB type gradient structure.....	36
Figure 4.8 Schematic of ABAB type gradient structure.....	36
Figure 4.9 Schematic of peripheral alignment of wires.....	37
Figure 4.10 Sandwich AABB gradient structure of FGM	37
Figure 4.11 Sandwich ABAB gradient structure of FGM	37
Figure 4.12 (a) Incremental gradient cold mounted sample (b) Sandwich gradient AABB etched sample.....	38
Figure 4.13 Electrolytic etching setup	39
Figure 5.1 EDS line scan of Incremental gradient FGM from bottom to top	41
Figure 5.2 EDS line scan region wise for elemental mapping.....	42
Figure 5.3 Top Region of incremental gradient FGM elemental mapping.....	43

Figure 5.4 Middle Region of incremental gradient FGM elemental mapping.....	43
Figure 5.5 Bottom Region of incremental gradient FGM elemental mapping.....	43
Figure 5.6 Optical image of the region 50%SS316L - 50%IN625.....	44
Figure 5.7 Optical image of the region 40%SS316L - 60%IN625.....	45
Figure 5.8 Optical image of the region 30%SS316L - 70%IN625.....	45
Figure 5.9 Microhardness of Incremental gradient FGM of total wfs 3.0 m/min.	46
Figure 5.10 Microhardness of Incremental gradient FGM of total wfs 4.0 m/min.	47
Figure 5.11 EDS line scan of Sandwich gradient AABB FGM from bottom to top	48
Figure 5.12 EDS line scan region wise for elemental mapping in AABB	48
Figure 5.13 Top Region of sandwich AABB gradient FGM elemental mapping.....	49
Figure 5.14 Bottom Region of sandwich AABB gradient FGM elemental mapping.....	49
Figure 5.15 EDS line scan of Sandwich gradient ABAB FGM from bottom to top	50
Figure 5.16 EDS line scan region wise for elemental mapping in ABAB	50
Figure 5.17 Top Region of sandwich ABAB gradient FGM elemental mapping.....	51
Figure 5.18 Bottom Region of sandwich ABAB gradient FGM elemental mapping.....	51
Figure 5.19 Optical Image at the top layer of ABAB structure	51
Figure 5.20 Optical Image between the layers at top in ABAB.....	52
Figure 5.21 Microhardness variation along the height of AABB FGM	52
Figure 5.22 Microhardness variation along with the height of ABAB FGM.....	53

LIST OF TABLES

Table 1 Conventional or Traditional manufacturing techniques for FGMs	5
Table 2 Chemical Composition of SS316L and IN625 (wt%)	27
Table 3 Optimised Process Parameters	30
Table 4 Layer by Layer wfs of the incremental gradient	32
Table 5 Design of experiment CCD approach parameters	58

ACRONYMS

FGMs	Functionally Graded Materials
AM	Additive Manufacturing
SL	Stereolithography
PM	Powder Metallurgy
ME	Material extrusion
MJ	Material Jetting
PBF	Powder bed fusion
DED	Directed Energy Deposition
EBM	Electron beam melting
SLS	Selective-laser-sintering
SLM	Selective-laser-melting
DMLS	Direct metal laser sintering
LENS	Laser engineered net shaping
WAAM	Wire Arc Additive Manufacturing
GTAW	Gas Tungsten Arc Welding
GMAW	Gas Metal Arc Welding
TIG	Tungsten inert gas
HAZ	Heat affected zone
LMD	Laser metal deposition
EDS	Energy Descriptive Spectroscopy
CNC	Computer numerical control
wfs	Wire feed rate
v	Deposition speed

Chapter 1

Introduction

1.1 Overview

Materials selection has become increasingly crucial and influential, despite various other constraints, as industries have developed, and new concerns and needs related to increasing productivity have emerged. It is easy to see how materials fitted to the requirements of each age have been attained one after another and, after a thriving period, have found a position compatible with modern and substitute materials. As a result, there are few advanced applications in today's world where a single material can go through all the service criteria, and creators are frequently obliged to combine materials. This search somewhat ends at Functionally Graded Materials (FGMs).

In 1986, Charles Hull developed the technology of Additive Manufacturing (AM) process Stereolithography (SL). Thus, it opens a new research area in manufacturing, enabling scientists to create other methods to develop the desired products. The unique kind of the AM process provides numerous benefits over traditional techniques. Complex components can be created in single step, exceptionally near the desired design, and with no limits of traditional manufacturing processes, using the AM process. Furthermore, reducing or minimizing the requirement to gather multi-component parts makes it feasible to decrease the quantity of part components in this procedure drastically.

1.2 Functionally Graded Materials

The enhancement of materials by each day to develop products with disciplined properties was produced when Functionally Graded Materials (FGMs) were offered for the first-time at manufacturing in research on producing materials for thermal confinement coatings in Japan,1984[1].

Since then, FGMs have become an academic research interest. Initially, these materials were built primarily to comply with the requirement of an extreme temperature situation and to minimize the stressed eccentricities[2]. In contrast, FGMs consider a class of cutting-edge engineering materials; the advantage of these types of materials is that a smooth, as well as sudden variation in properties and its behaviour in one or more, desired directions due to the alteration in chemical composition and microstructure, which can efficiently enhance the functioning and facility life of the functionally graded materials[3]. We come across several materials like these in our day-to-day life; Bones, Skin, and Teeth are some of the natural examples. FGMs can strengthen discrete materials and offer a unique solution for creating components that work in challenging situations. FGMs applications have matured in current years, and there is a growing demand for FGM applications. Most of the uses of FGMs emerges from their ability to be adjusted to satisfy the needs of different characteristics in different places within a single part. FGMs were primarily utilised in aircraft, but its uses have spread to various industries, as seen in Figure 1.1 [4].

FGMs are categorized as continuous or discontinuous, as shown schematically in Figure 1.2 a) and b) compositions and/or microstructures vary in a stepwise manner in discontinuous FGMs, normally with the occurrence of a boundary. Continuous FGMs, on the other hand, have compositions and/or microstructures that change with position. Figure 1.2 c)–h) are schematics depicting various FGMs. In addition, graded structures can be found throughout the material or in specific areas of FGMs. Moreover, graded structures are present either throughout the entire material or only in some localized regions[5]. Manufacturing processes play a crucial role in achieving the geometric features, chemical composition, and microstructure requirements of gradient structures, and hence the qualities and performance of FGMs. Additionally, deciding the production method is vital based on economic (cost and time) and environmental considerations (consumption and pollution).

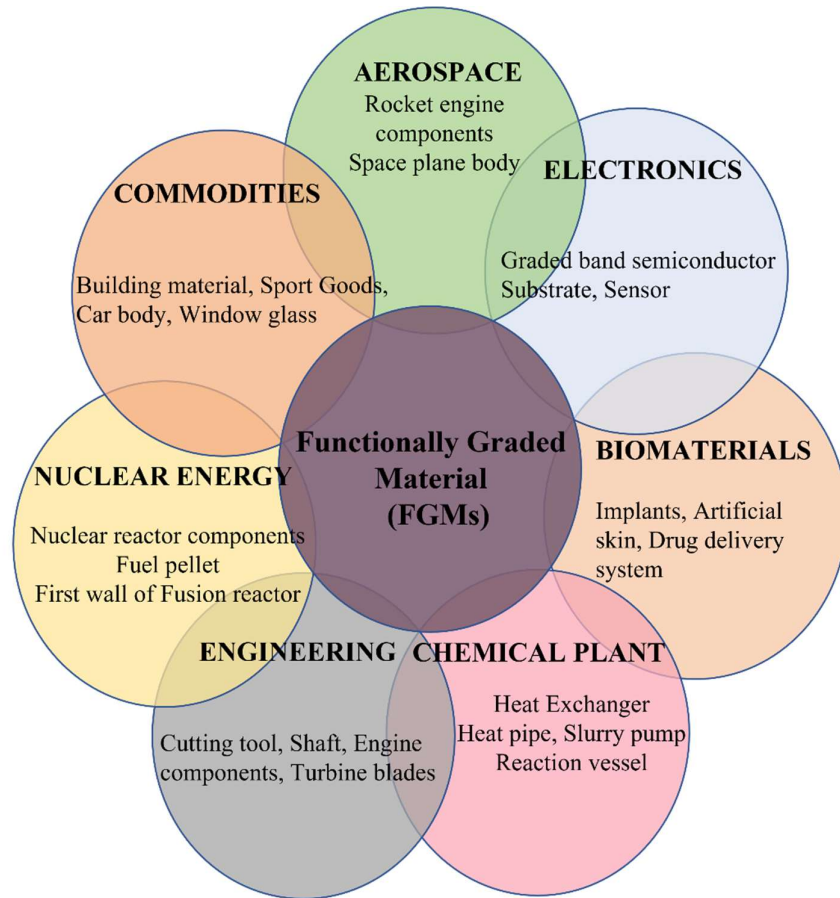


Figure 1.1 Applications of Functionally Graded Materials [4]

FGMs are classified into two types based on their geometry: thin film or coating and bulk. Gas-based technologies, as well as other processes, are utilized to develop thin film or coating FGMs [6]. There are two types of processing procedures that can be utilized to make bulk FGMs: liquid and solid phase approaches. Table 1 summarizes the processes used to make thin film or coating and bulk FGMs [7-12].

1.3 Manufacturing Methods of FGMs

In this section, the types of manufacturing methods will be discussed in detail with their pros and cons.

1.3.1 Conventional Techniques

Over the last thirty years, the processes for generating FGMs have been studied, and there are currently several advances employed in the production of these FGMs. Examples include centrifugal methods, powder-based methods, vapor deposition methods, and solid free-form fabrication methods. The prime reason for the development of a newer technologies for producing FGMs is that these materials have extensive properties and are required by a variety of desired applications [13].

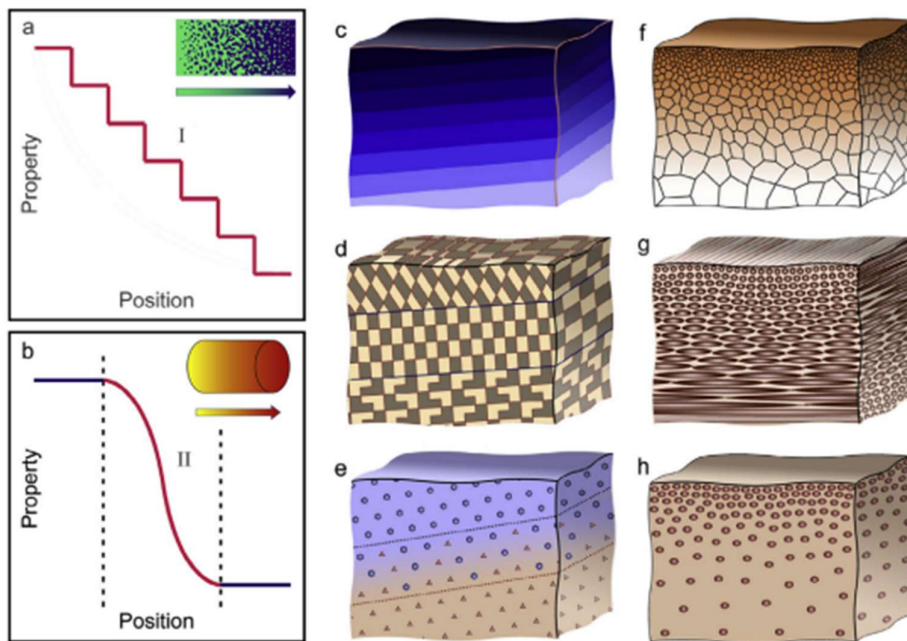


Figure 1.2 Schematics of different types of FGM [5]

The above-mentioned methods can broadly categories into two methods Conventional or Traditional techniques of manufacturing and New- Age Technique Additive Manufacturing (AM).

In conventional or traditional manufacturing processes for FGMs the processes include powder metallurgy, centrifugal casting, thermal spraying, spark plasma sintering, chemical/physical vapor deposition (CVD/PVD), sheet lamination.

Table 1 Conventional or Traditional manufacturing techniques for FGMs

Category	Method	Type of FGMs
Gas-based method [7–10]	<ul style="list-style-type: none"> • Physical vapor deposition • Chemical vapor deposition • Surface reaction process • Thermal spray 	Thin film or coating
Solid-phase process [7], [8]	<ul style="list-style-type: none"> • Spark plasma sintering • Powder metallurgy 	Bulk
Liquid-phase process [7], [8]	<ul style="list-style-type: none"> • Centrifugal casting • Gel casting • Slip-casting • Electrophoretic deposition • Directional solidification • Sedimentation • Tape-casting 	Bulk
Other methods [7], [8], [11], [12]	<ul style="list-style-type: none"> • Electrode deposition • Ion beam assisted deposition • Plasma spraying 	Thin film or coating

The following is a description of the centrifugal casting technique used in the manufacture of FGMs. To begin, the second phase (i.e., reinforcement) is mixed into a molten metal to create a homogenous combination. The gradient in the volume fraction of the second phase is then established and maintained by directing the solidification process using gravitational/centrifugal forces [14]. Despite the possibility of mass production, accurate control of the second phase distribution provides a significant difficulty. Furthermore, while the gradient is generated through a "natural" segregation process, the mechanism behind the centrifugal approach limits the capacity to alter the resultant microstructure and hence the types of gradients that can be designed.

Although the centrifugation approach can make continuous FGMs, it is only capable of producing FGMs with radial gradients [15]. Vapor deposition is commonly employed in the fabrication of thin FGM. Because of the high energy consumption and long process, it is not a cost-effective method of producing bulk FGMs while the centrifugal casting can only produce the cylindrical parts [16].

However, published data indicate that FGMs made employing Powder Metallurgy (PM) methods nearly invariably have a handful of pores, which effectively decrease the thermal, mechanical, physical, wear, magnetic, and corrosion properties [17]. Due to laser control, laser deposition produced parts have exceptional accuracy. Material that is selectively deposited reduces post-process machining/finishing. FGMs in quantity is uneconomical. It produces only discrete structures in which post-heat treatment is required when residual stresses are relatively substantial [18].

Conventional methods for producing FGMs can only produce items with simple shape, with low dimensional accuracy, and the output usually requires further treatment. Given the limits of existing or conventional methodologies for the manufacturing of FGMs, the development of AM technologies has piqued the curiosity among many.

1.3.2 Additive Manufacturing (AM)

Additive Manufacturing (AM) is a solid-freeform manufacturing method that allows for the through creation of finely comprehensive bespoke components by precisely positioning material in a design domain. As manufacturability has improved, AM technologies have progressed from manufacturing one-off prototypes to producing full-scale end-use items. Because of the technological advancements in today's AM systems, it becomes the novel method for the fabrication of the Functionally graded materials (FGMs) can be done efficiently and effectively.

AM is stated by ASTM as "the technique of combining materials to produce objects from three-dimensional model data, often layer over layer, as opposed to subtractive manufacturing methodologies." [19] This fabrication approach has several advantages over typical subtractive manufacturing techniques, including a reduction in the quantity of material required to manufacture a comparable component. This enables the fabrication of more complicated components in a single build and minimises the amount of connecting of individual components required, hence reducing areas of weakness in a finished part.

According to the ASTM the AM methods broadly comes into 7 categories based on the feedstock, technique of deposition, energy source and the type of material.

1. Binder Jetting

The principal of binder-jetting method based on ink-jet technology, 3D printing, was invented at the MIT, USA. Drops of a binder substance are accumulated over the base of a powder bed in this procedure, adhering the powder particles at the same time where the component is to be formed. The process is then repeated by reducing the powder bed with a piston, spreading a new layer of powder over the former layer, and depositing binder over the surface of the fresh layer. This method is repeated until the entire portion is completed. However, because of the very partial types of binder given by the nozzles, the capacity of multi material additive manufacturing applying this approach is low, unless the powder-bed substances can be modified using another dry powder distributing technology [20].

2. Photopolymerization Vat

Using various types of light sources, photo-polymer vat techniques involve selective curing of pre-deposited photo-polymers. Stereolithography (SL) is the most common photo-polymer vat process, which involves projecting a cross section of a particular slice of an object over a photo-sensitive liquid polymer, solidifying each photo-polymer

layer. The platform within the photo-polymer vat moves down the solid section of the photo-polymer, and the laser traces out the next layer of uncured photo-polymer. This technique is repeated until all the layers of the whole construction have been built. Scanning SL and projection SL are the two basic SL techniques developed for distinct beam delivery systems. The main advantages of the various material scanning SL method are its high surface finish quality and dimensional precision [21]. It also provides a diverse selection of polymers for embedding various colors in medical prototypes and tailoring bioactive and mechanical qualities in tissue engineering uses. The system may generate various material things with horizontally & vertically oriented edges. On the other hand, contamination is difficult to eradicate using this method. It has received widespread interest from various industries, including metamaterial, footwear, jewelry, and biomedical engineering [22].

3. Material Extrusion (ME)

Material extrusion is the most extensive installed base among AM methods. ME machines construct structures by pressing material through a nozzle in a regulated manner. The buildup material is often a polymer filament squeeze out through a heated nozzle, an automated edition of the arts and crafts hot-glue gun. The platform either travels down or the nozzle moves up after the nozzle drops a layer of metal onto a platform, and a new layer of material is deposited. When two nozzles are put in a machine, one of them is commonly utilised to deposit a water-soluble substance. In machines developed for tissue engineering research, three or more injectors or nozzles are sometimes employed to deposit scaffolds and other biologically suitable materials specified parts of the implant [23].

4. Sheet Lamination

Sheet lamination procedures construct an object by cutting and stacking sheets of material. This method has been used to construct wood-like metal components and plastic structures using paper, plastic, and metal sheets. Paper and plastic sheets are usually bonded using a binder,

whereas metals are typically bonded via welding (thermal brazing or ultrasonic welding) or bolting the sheets together. Sheet lamination has also utilised with ceramic and metal green tapes (e.g., powder held together by a polymer binder in the shape of a material sheet) to construct structures later burned in an oven to generate an impenetrable part [24].

5. Material Jetting (MJ)

Material jetting AM techniques directly layer wax and/or photo-polymer droplets onto a base using drop-on-demand ink jetting, like inkjet print technology that transports ink droplets from a fluid channel onto a paper base in a dip-by-dip manner. Heating or photocuring causes the blasted droplets to change phase. However, the suspensions have a low intensity of solid elements because to the viscosity restrictions of the processing fluids used in ink-jetting [25]. The MJ technology is a popular additive manufacturing approach in the polymer printing industry due to its benefits over other polymer printing processes. Thanks to technology, we can adapt tiny layer thicknesses, allowing us to print high-quality parts with less noticeable staircase effects and thin wall features. This approach can be utilised to design complicated FGMs with gradient compositions in several directions since the kind and number of raw materials sprayed by printheads can be quickly and flexibly modified. However, this method generates much waste because the materials needed to build the substrate and those removed during nozzle cleaning are thrown away. Typically, materials made using this approach, particularly FGMs, have more defects than materials made using other methods [26].

6. Powder Bed Fusion (PBF)

The powder bed shields the molten metal in an inert environment or partial vacuum. To selectively melt the material according to the part cross-section derived from the digital part model, an energy source which can be either laser or electron beam is used to scan every layer of the already scattered powder. When one surface is inspected, the piston

in the buildup chamber descends, and the piston in the powder compartment ascends by the layer thickness defined. The coating mechanism, also

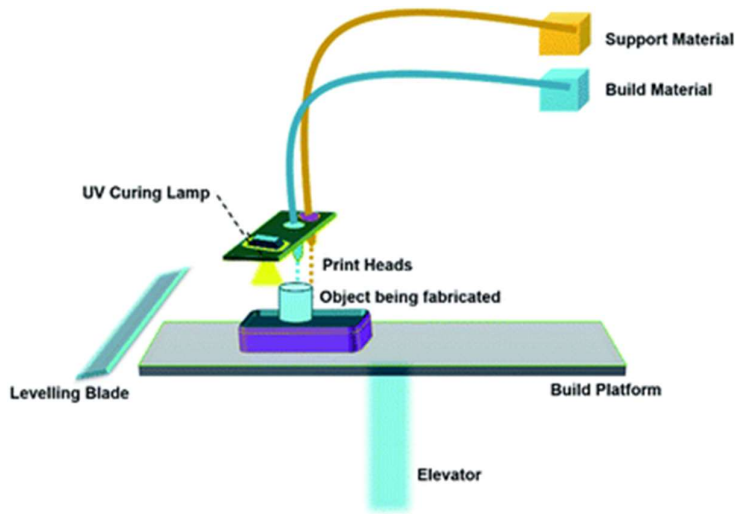


Figure 1.3 A schematic representation of the material jetting process. [26]

known as a roller, spreads powder across the build compartment, which is then scanned by the radiation source. Layer by layer, this procedure is continued until the entire part is created. This is a powder cake procedure, so the part won't be seen until the extra powder is removed. PBF-based methods require more time to produce a part than DED technologies, but they can achieve higher complexity and better surface finish with minimal post-processing. Multiple parts can be built together to utilise the building chamber fully [27]. (i) Selective-laser-sintering (SLS), (ii) electron-beam-melting (EBM), (iii) selective-laser-melting (SLM), and (iv) direct-metal-laser-sintering (DMLS) are examples of powder bed fusion printing processes. SLS is a 3-D printing technology that uses a carbon dioxide (CO₂) laser beam to sinter powder. The enclosure is heated to just below the substance's melting point. The laser fuses or melts the particles layer by layer at the surface. Each time a layer is finished, a piston controls the layer thickness to guarantee that each

layer is the same thickness. Styrene, acrylic, and nylon are polymers that could be employed and metals like copper and composites like polyamide with fiberglass. PBF procedures are appropriate for functional Multi-Material AM parts that require a broader range of materials and material qualities than standard manufacturing methods can provide.

7. Directed Energy Deposition (DED)

In this process the focused thermal energy i.e., either in the form of laser, in form plasma arc or electron beam which is used to dilute the materials by melting them and as they will be depositing over the substrate or another layer. There is various process that comes into DED mainly Laser engineered net shaping (LENS), Direct-metal-transfer (DMD), and many more. The DED processes are giving priority when it comes to fabricate the functional grading materials due to their low feedstock losses. The potential problem in dis-similar additive manufacturing of materials by DED is formation of intermetallic phases which formed as it is fusion-based process. The DMD or WAAM process further split into three different types of methods as the wire arc additive manufacturing (WAAM). Those process is explained more in detail in next section.

1.4 Wire Arc Additive Manufacturing (WAAM)

The fastest growing manufacturing processes that are useful from the perspective of the manufacturing industry is arc-based processes. The main reason is the metal components can be fabricated with lower cost with the desired design and there is very less loss of feedstock, and the production time is very short compared to the conventional manufacturing process. WAAM fabricated products have good mechanical properties as the materials during deposition gets melted and then solidify to get deposited [27]. The process has been effectively employed in manufacturing or fabricating products with many materials such as stainless steel, titanium, nickel and its super alloys, aluminum, etc. In WAAM, the heat source is generated by electric arc and then the metal wire is fed into the arc and build a part layer by layer [22]. With WAAM we can fabricate the large components even a space rocket is already built by velocity. The advantage of this process is large deposition rate. WAAM process can further bifurcate into three commonly used methods like

- Plasma Arc Welding (PAW) in this process the arc is generated by plasma and the wire is feed into arc to build the part.
- Gas Metal Arc Welding (GMAW), the consumable electrode as wire is used to generate arc at the electrode and feeding of the wire should be continuous to build the part.
- Gas Tungsten Arc Welding (GTAW), the electrode used in this process is non-consumable and the arc is at the substrate then wire is feed into arc to fabricate the part.

For the fabrication of FGMs the most suitable method is WAAM, but for feeding the dual wire simultaneously into the arc this where the GTAW based WAAM edged over the other WAAM process.

GTAW based WAMM can be abbreviated as WAAM-TIG. The process allows to use the multiple wires to feed into the arc. Also, most of the energy is went to substrate to form HAZ, to utilised the

unused arc energy another wire can be feed to increase the deposition rate. Further in-depth study and experiments are performed in this research work.

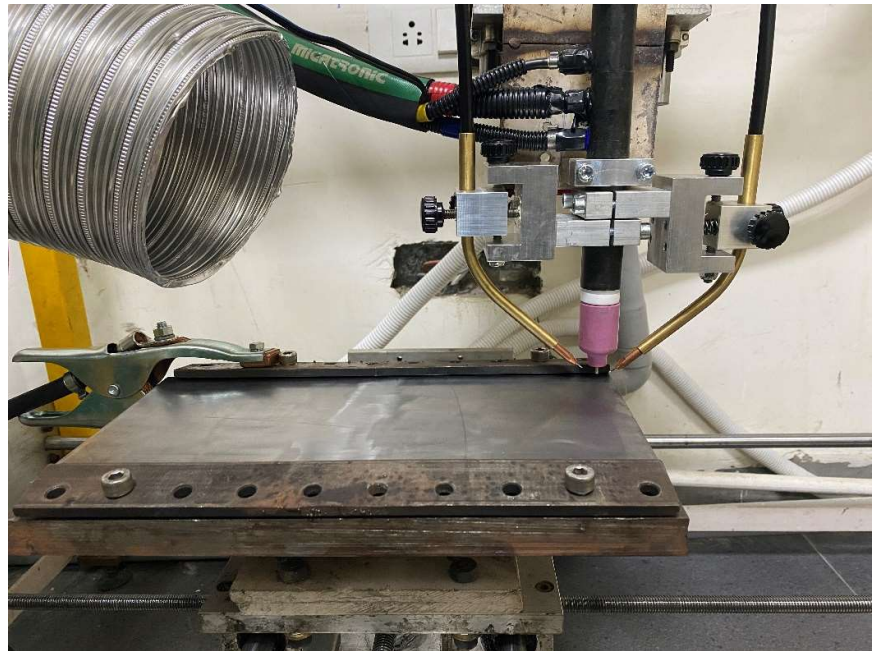


Figure 1.4 WAAM-TIG setup with dual wire feeding nozzles

In the Figure 1.4, a Tungsten electrode is inside the torch with dual wire is kept at 120° with each other and at an angle of 45° with the substrate to conduct the smooth flow of materials into the melt pool. The exhaust pipeline is to take away the harmful gases released during the fabrication.

1.5 Organisation of Thesis

Chapter 2 gives the preview and research about the topic and detailed literature review of the past work into the field of additive manufacturing and fabrication of FGMs and based on that the materials selection with the objective for this research work.

Chapter 3 it includes the experimental setup and process parameter optimisation which is used for fabrication of FGMs.

Chapter 4 presents the design of the various FGMs which are proposed for this research work. Further research methodology is established to maintain the flow of work and analysis with characterisation techniques.

Chapter 5 includes the results from EDS, Optical images of the microstructures, hardness measurements.

Chapter 6 highlights the conclusion of the present research work and marks the future scope of work in this field to enhance the properties of the FGMs.

Chapter 2

Literature Review and Objective

2.1 Overview

In this section, the work of the various researchers and scientists is discussed and reviewed. There is lot of work going on the fabrication of FGMs and its mode of manufacturing here we mentioned that are related to our interest either in terms of materials or in terms of deposition method.

2.2 Literature Review

Carrol et al. investigated SS304L-IN625 FGMs by lowering SS304L vol. by 4% and increasing IN625 vol. by the same amount in neighbouring deposits. When the content of SS304L is greater than 85%, the structure changes gradually from austenite and ferrite to columnar dendrites when the range of IN625 is greater than 50%, passing through a cellular grain that is distinctive to the gradient zone. Due to creating a secondary phase, cracks were discovered in the grading zone when SS 304L was around 82%. The CALPHAD approach is used in this work to effectively estimate the constancy of crack generating secondary phases at varying concentrations along the gradient. To forecast and understand the property of progress along the gradient, a vital technique for integrating experimental characterization with computational thermodynamics is built [28].

Meng. W et al. fabricated and studied an FGMs that grades from SS316L to IN625, manufactured via fiber LMD and laser-based synchronous pre-heating. With non-preheating and preheating settings, the microstructure evolution, microhardness, and cracking behaviour of the FGM were by experimentation investigated as an act of position. Under non-preheating situations, the formation mechanism of neighbouring cracking for gradated deposits was observed and further investigated. Figure 2.1 shows the crack when the wt% of SS316 is

nearly 90 in non-preheated FGM. The main cause of cracking has been found as the precipitation of Mo and Nb-enrich phases. The Microhardness of the fabricated FGMs showed a nearly linear distribution in the gradient direction and the maximum tabulated at the 100% IN625.

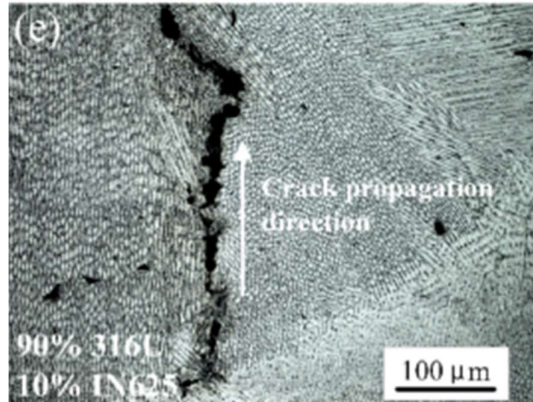


Figure 2.1 Crack at 90%SS316L-10%IN625 in a non-preheated sample.

Finally, the feasibility of gradient forming from SS316L to IN625 using fiber LMD and a laser-based synchronous pre-heating method was established to fabricate the FGMs without any cracks [29].

Chen et al. manufactured the FGM of SS316L and IN625 with laser-direct-metal-deposition (LDMD) and analysed the microstructure of the fabricated FGM components was compact, with consistent composition change along the graded direction. The primary dendrites turn out to be fatter, and gap between them became more significant as the IN625 content increased, and the heat accumulated. The white following phases appeared along the dendrites border when the IN625 content surpassed 80%. During laser deposition, Mo and Nb atoms diffused from the solidification head to the liquid-zone, this aided in creating eutectic and NbC phases. NbC was difficult to generate in the deposition layers adjacent to the substrate due to the rapid solidification time and quick cooling rate. The strengthening impact of Mo, Ti, and Nb became increasingly apparent as the IN625 concentration grew and the amount

of hard phase expanded, lowering wear of material and improving the wear resistance of FGM of SS316L-IN625 [30].

Shah et al. worked on gradient laser deposition between SS316L and IN718. Although fusion welding is commonly used to combine these alloys, the weld material and HAZs are especially prone towards solidification cracking. Composition effects dominate the cracking mechanism; alloying materials and impurities are segregate to interdendritic sections, causing low-melting liquid layers to endure across grain boundaries. Such structure consequences are tough to avoid, although simple grain bulk optimisation has been demonstrated to reduce cracking. Unlike traditional welding, the scientists highlight that LMD of these connections provides a unique chance to enhance process variables to stimulate grain refinement. Low laser powers were discovered to result in quicker cooling rates and a thinner microstructure; however, impact of this laser based deposited microstructure on solidification cracking was not explicitly examined. The power and powder mass flow rate influence secondary-dendritic-arm-spacing (SDAS). The formation of carbides such as NbC at greater IN718 concentrations allows for selective control of the functional material's hardness and wear resistance [31].

Wang et al. investigated and performed the AM of IN625 based on WAAM-TIG, wherein the near to the substrate area, IN625 is composed of cellular grains with no secondary dendrites, In the layers, columnar dendrites directed upwards, and in the top region, a transition from oriented dendrites to equiaxed grain. The fabricated additive manufactured part the segregation behaviour of alloying components like Mo & Nb intensifies with increasing deposited height, with maximum development in the top area. The major dendrite arm spacing is coherent with laves phase content. Tensile strength and microhardness vary significantly among areas. The near-substrate region has higher tensile strength and microhardness than the layer and top part. The growth of columnar dendritic epitaxially from the base is revealed by the peaks detected in XRD analysis [32].

Kim et al. fabricated and investigated the FGMs with a distinct composition range of IN718/SS316L was fabricated using DED and laser as the power source and powders as feedstock. It was discovered that crucial flaws were developed in the regions of 30% IN718/70% SS316L and 20% IN718/80% SS316L by wt%. The spectroscopic results, microscopic images taken by optical microscope, and mechanical investigations of the fabricated FGMs indicated the reason and method of such faults were developed. The imperfections were formed by three types of complexes, according to the results of spectroscopic analyses and microscopic: (i) ceramic oxides like Al_2O_3 and TiO_2 produced via oxidation in high-energy laser irradiation, (ii) precipitates with the same chemical compositions, and (iii) segregants; the latter two were distinguished due to variances in their shape, size, and spreading in the microstructure of the IN718/SS316L. Smaller unevenly shaped segregants generally found in the inter-dendritic part, while bigger precipitates were mostly found along grain boundaries. The problematic composition of sections where the hot cracking occurrence was most to be expected to occur were purposefully and intentionally disregarded, while the remainder of the FGM was held. The DED procedure improved the bond-ability of IN718 and SS316L, which had previously been challenging to combine directly using traditional methods [33].

The steady changes in composition, micro-structure, and characteristics of smooth gradients, where lower stress throughout the evolution zone compared to conventional welding, are one advantage of AM-FGM over the welding. The automotive engine valve stem is a brilliant example of this comparison. These automotive engine valves are commonly friction-welded from a elevated-temperature Ni-based alloy (like IN625) & an SS304L stem. The rapid shift in the interface is most likely what caused the welded joint to fail. **Hofmann et al.** created a FE model for a gradient alloy part. The graded joint has a tenfold lower stress concentration, according to the model. This is due to the gradual shift in the coefficient of thermal expansion, which results in reduced residual

stress. Furthermore, the fast change in welding might promote the production of unannealed intermetallic, weakening the joint even more.

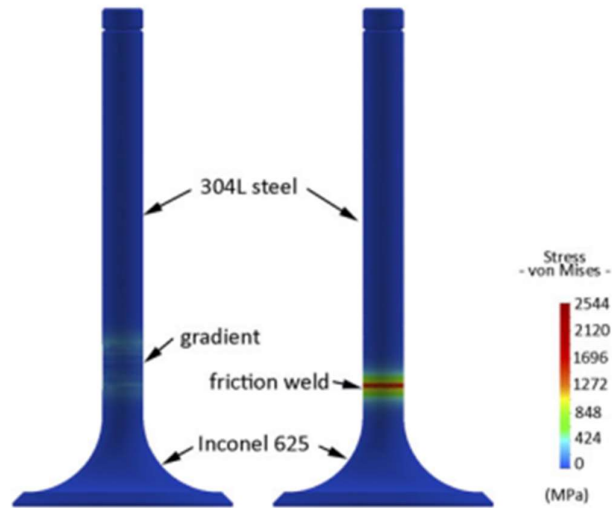


Figure 2.2 A FEM model of gradient alloy automotive valve stem [34]

Figure 2.2 illustrates a FE model of an automotive valve stem, which is an example of a part that can benefit from a gradient alloy. The length of the gradient region between SS304L and IN625 is 2.5 cm. And the entire part is turned out to be a single phase of austenite. According to the model due to the paucity of thermal expansion, the connection with the gradient alloy has a tenfold smaller stress at 1000 K. Due to thermal expansion, the gradient juncture has an order of scale smaller tension at 1000 K. The friction welded part has stress at the joint is roughly ten times greater than the compositionally graded alloy [34].

Kumar et al. fabricated the FGM of IN625/SS321 using the WAAM-MIG process and examined the subsequent mechanical integrity and microstructure features. The fabrication done by WAAM-MIG was successfully performed to produce FGM without any cracks. The structure of FGM was deposited so that few initial layers were of SS321; after that few layers of IN625 were deposited. The microstructure of SS321 was mostly austenitic, with a significant amount of δ -ferrite

inside the austenite matrix, whereas Inconel 625 was entirely austenitic with a laves phase. The microstructural features varied depending on the build direction, with columnar dendrites and equiaxed in the SS321 region and fine, cell-form, and columnar dendrites with secondary arms and precipitates in the IN625 layers.

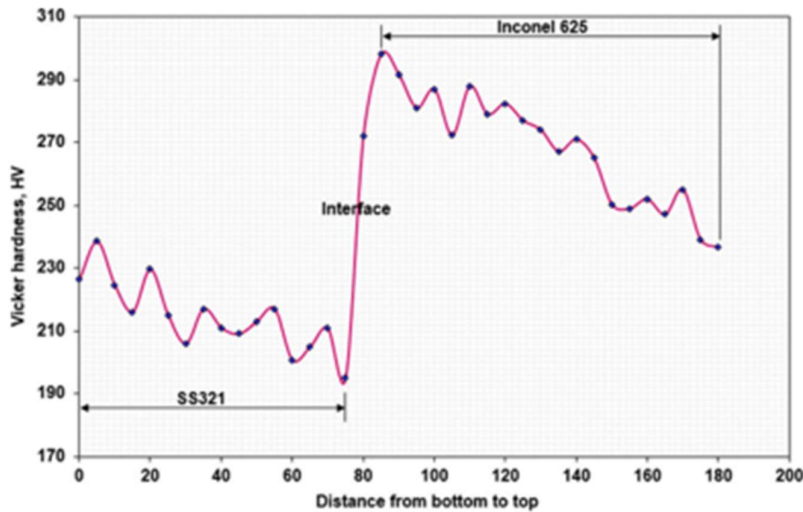


Figure 2.3 Microhardness variation of FGM from bottom of the SS321 to the top of IN625

In samples of IN625, Mo and Nb precipitates were found. In the SS321 and IN625 areas, the microhardness values continuously declined from bottom to interface and interface to top as deposition height increased Figure 2.3. The microstructural variation along the constructed direction causes the change in microhardness. Because of the identical crystal structure-FCC, EBSD testing revealed that the preferred grain growth direction in the interface without grain growth discontinuities was $\langle 001 \rangle$. The movement of alloying elements in between two alloys was confirmed by EDS analysis, and laves phase was observed in the interdendritic areas of IN625 layers [35].

Zhang et al. , investigated and fabricated the FGMs of SS316L/IN625 and deposited 100% SS316L and 100% IN625 (Figure 2.4) using laser-based DED, and quantitative analysis, microstructure characterisation,

hardness measurement, and tensile testing were performed on the planned samples.

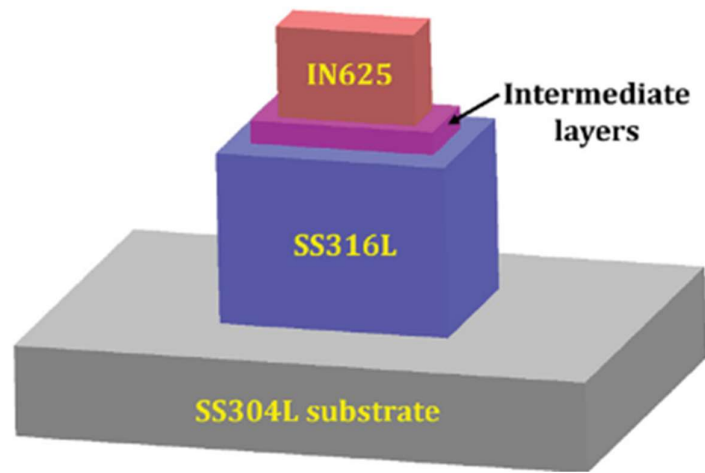


Figure 2.4 A schematic of FGM (SS316L-IN625)

All the deposits are observed on a micrograph where no cracks, pores or un-melted particles were seen. EDS line scan from the bottom (SS316L) to top (IN625) of FGM shows the difference of Ni & Fe content varying gradually, suggesting the productive production of the gradient material. Microhardness measurements for 100% SS316L and 100% IN625 reveal that microhardness increased sharply at the interface. Hardness values transversely the gradient part of gradient samples were observed to steadily move from the Stainless steel 316L side to the Inconel 625, as it can be seen in Figure 2.5. Gradient specimens cracked at the SS316L part, whereas both interfaces (SS316L to intermediate layers-intermediate layers to IN625) endured the tests, according to tensile fracture morphology and elemental mapping. Because IN625 has a substantially higher yield strength than SS316L, necking is primarily found in the SS316L and gradient zones. For 100% SS316L and IN625 fabricated parts, microstructure analysis revealed a sudden transformation of the structure at the dual-material boundary. The microstructure of gradient samples gradually evolved from cellular on the SS316L side to a blend of cellular & columnar structures on the

adjacent layers, and ultimately to primarily columnar on the Inconel 625 [36].

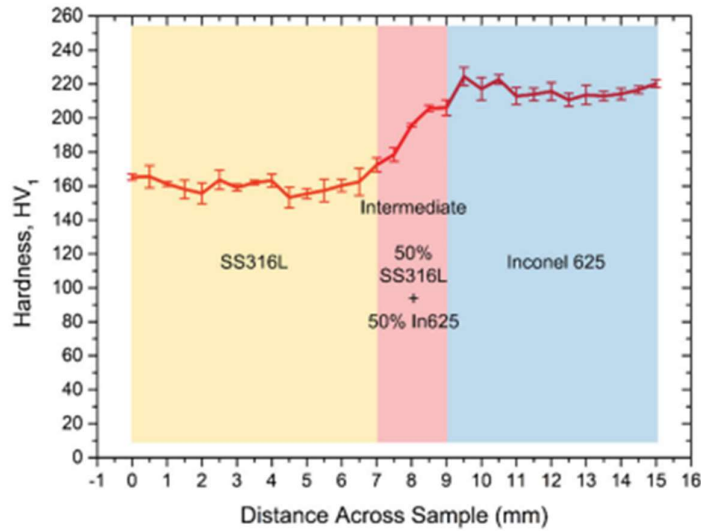


Figure 2.5 Hardness (Vickers) measurement of FGMs

After the above section, we can conclude the difficulties and precautionary measures for fabricating the FGMs of SS316L and IN625. Occurrence of a crack in the region where Fe content is higher. Microstructure characterisation, mechanical properties analysis like hardness measurement, tensile testing, and wear resistance analysis will give the idea about the fabricated FGMs. Thus, WAAM-based TIG will be more feasible to fabricate the FGMs of SS316L and IN625.

2.3 Objectives of the Present Research Work

- To establish the functionally graded material of varying combinations of SS316L and IN625 using the WAAM process: WAAM-TIG shall be developed utilising two independent wires.
- To investigate the different possible approaches to fabricate FGM, such as Sandwich-like structure and variable gradient FGM: deposition of two wires simultaneously by feeding it through individual cold wire feeder.
- Optimisation of process parameter such as arc current, deposition speed, and individual wire feed rate will be performed.
- To study the percentage dilution: EDS scan to be performed to analyse the gradient variation of key elements such as Fe, Ni and Cr. Line scan across the height of the sample with the elemental mapping across the different interfaces.
- To study the mechanical proprieties: analysed by studying the microhardness variation across the height of the deposited bead.
- Microstructure analysis of variation at the interface and over the height.
- To achieve the mini. The wire feed rate to have a proper deposition.
- Effect of variation of process parameters:
 1. Weld Bead and Weld Height
 2. EDS line scan
 3. Hardness Measurement

Chapter 3

Experimental Setup and Parameter Optimisation

3.1 Overview

After getting familiar with the FGMs and their fabrication processes like conventional techniques and additive manufacturing methods, and their pros and cons now, in this chapter, we will discuss the experimental setup of WAAM-TIG and the perform the optimisation of the parameters such as current, wire feed rate, and deposition speed. Further, fabricate the FGM structure with different compositions of SS316L and IN625.

3.2 Experimental Setup

The WAAM-TIG setup used for smooth conducting of this research work and the fabrication of FGMs was in-house developed where all the three-axis have a linear motion, and the programmable controlling unit is integrated with the system for the automation[37]. The fixture for positioning of dual-wire is in-house designed and fabricated to make the system steady.

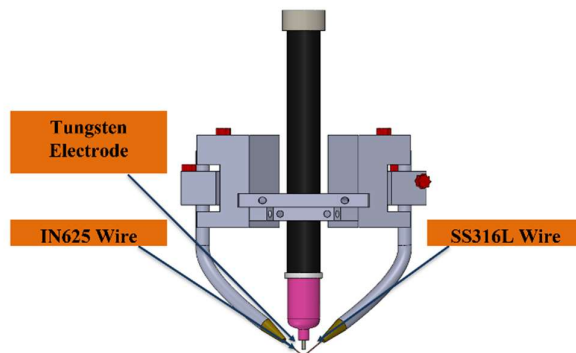


Figure 3.1 Pictorial Representation of Dual wire fixture setup

WAAM-TIG setup where at the center a substrate holder is mounted on the asbestos bricks Figure 3.1 shows the deposition is done on WAAM-

TIG in which both the wires are feeding together with different nozzles. The electrode diameter (D_e) is 2.4 mm, and the stand-off distance (SOD) is kept at 4 mm throughout the experiment.



Figure 3.2 Migatronic TIG (350 AC/DC) power source

The materials opted for this research work are SS316L and IN625 with a wire diameter of 0.8 mm the chemical composition of both wires is shown in Table 2.

In Figure 3.2 the shown WAAM-TIG power source used in work is MIGATRONICS (PI 350 AC/DC), and the computer system controls the movements of the CNC with the automation.

Table 2 Chemical Composition of SS316L and IN625 (wt%)

Alloy	Elements												
	Fe	Ni	Cr	Mo	Mn	Si	C	P	S	Al	Ti	Co	Nb
SS316L	Bal.	12	17	2.5	2	0.75	0.03	0.045	0.03	-	-	-	-
IN625	2.5	Bal.	21	9	0.5	0.5	0.1	0.015	0.015	0.4	0.4	1	3.6

A dual wire-based WAAM-TIG setup consists of a three-axis line motion-based CNC machine, Tungsten electrode holder, wire feeder fixture, spool of wires of the material SS316L and IN625 for the continuous feeding of the wire, cold wire feeder, exhaust pipe, and continuous supply of 100% Argon gas the equipment as mentioned earlier and machines shown in Figure 3.3.

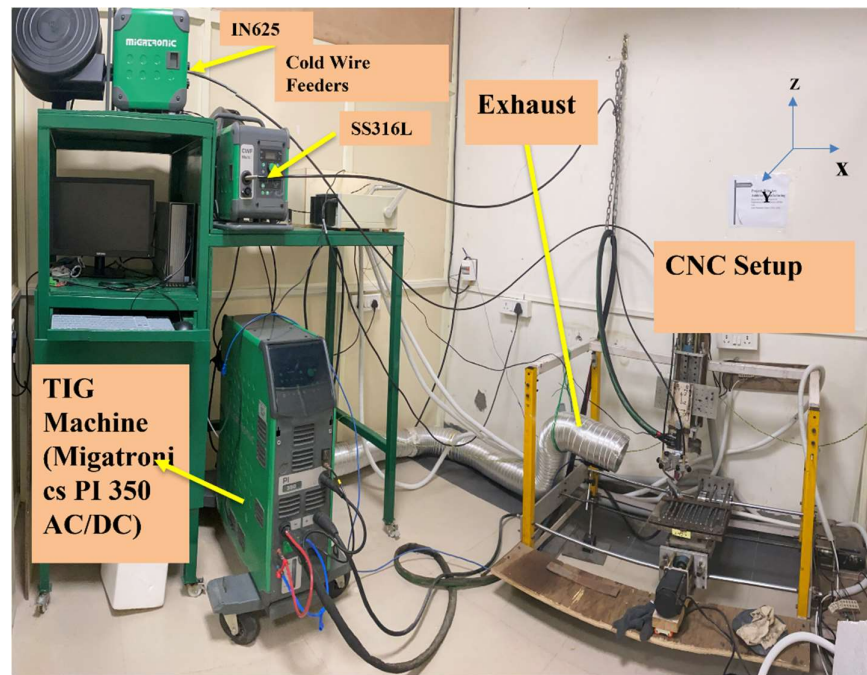


Figure 3.3 An experimental setup of WAAM-TIG

3.3 Optimisation of process parameters

One of the objectives is to get the minimum wfs of a single wire so that deposition should be uniform through the length of the deposited bead. To achieve the minimum wfs and smaller HAZ, the arc current and deposition speed play a vital role and the alignment of both the wires. The alignment of the wires should be at the center of the electrode and simultaneously align at the bottom center of the tungsten electrode to get the bridge transfer deposition of the materials.

To optimize the minimum wfs we first sorted out the current and deposition speed (v) for the maximum wfs we required i.e. 4 m/min or 3 m/min.

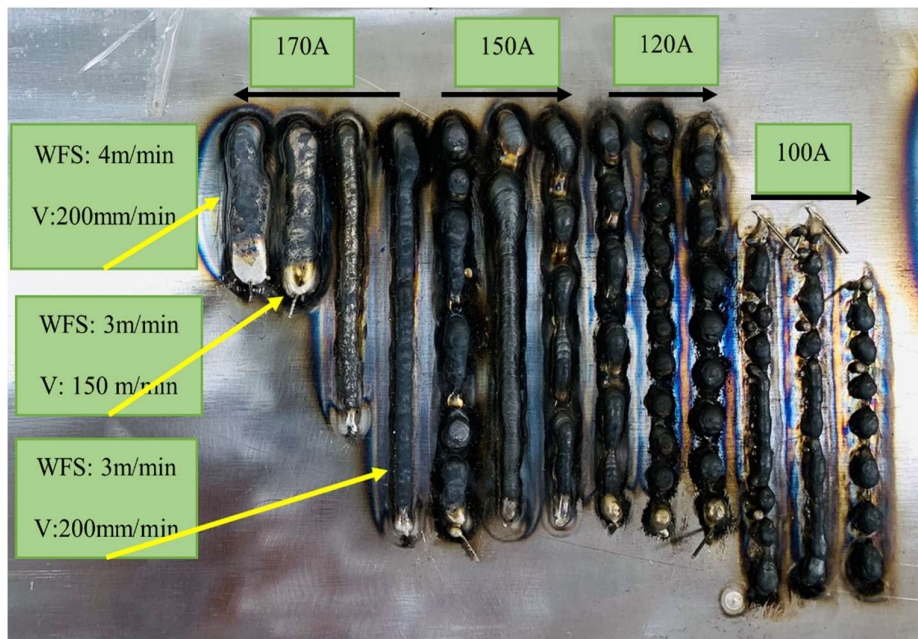


Figure 3.4 Process parameter optimisation for maximum wfs.

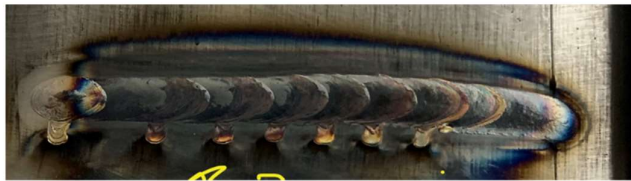
Thus, the heuristic approach is considered to get the current and deposition speed.

After depositing the material with the same current and varying the speed to get the optimised current, and then by varying the wfs and deposition speed, we get the optimised deposition speed for the maximum wfs.

Figure 3.4 shows the parameter variation and the deposited bead to optimize the process parameter. To get the minimum wfs we must put the same current (170A) and the deposition speed (200 mm/min), then go for the minimum wfs.



(a) $I=170A$, $V=200\text{mm}\backslash\text{min}$, $wfs=0.2\text{m}/\text{min}$



(b) $I=170A$, $V=200\text{mm}\backslash\text{min}$, $wfs=0.3\text{m}/\text{min}$



(c) $I=170A$, $V=200\text{mm}\backslash\text{min}$, $wfs=0.4\text{m}/\text{min}$

Figure 3.5 Optimisation for minimum wfs

In the above Figure 3.5 (a) the deposited bead is not uniform compared to the (b) and (c). Thus, process parameters for fabrication of FGMs having SS316L and IN625 with WAAM-TIG have been optimised for this research work and tabulated in **Table 3**. As the process parameters are now optimised, the fabrication of FGMs of SS316L and IN625 should start. To fabricate the FGMs, the two types of structure is designed and finalised, incremental gradient and sandwich structures.

Table 3 Optimised Process Parameters

WAAM-TIG Process Parameters

I (A)	v (mm/min)	wfs (m/min)	D _e (mm)	D _w (mm)	SOD (mm)	Shielding Gas
170	200	4 and 3	2.4	0.8	4	100% Argon

In the next chapter, fabrication and analysis of the deposited FGMs will discuss, along with the mechanical and microstructure analysis.

Chapter 4

Design and Research Methodology

4.1 Overview

The experimental setup and the fabrication and production of the FGMs can be done with automation with optimized parameters. In this chapter, we will fabricate the two types of FGMs i.e., Incremental gradient structure and Sandwich gradient structure, and set the research methodology of its EDS, Optical Micrograph, and the Micro-Hardness analysis to perform along with the height of the deposited FGM.

4.2 Incremental Gradient Structure

The design opted for this research work is 10% incremental gradient structure where the SS316L will be 100% at the bottom and after every 2 layer the decrement of 10% in SS316L and simultaneously increment of 10% in IN625 will be there as per the design. This can be visualised in the Figure 4.1 shown below.

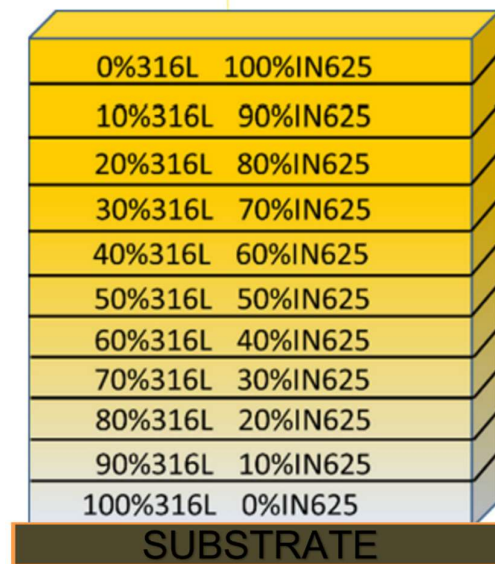


Figure 4.1 A schematic of the Incremental gradient structure of FGM

To maintain the composition of both the materials so that they will be deposited in a controlled manner. We can control the wfs of both the wires. In this case, we went with the two values of total wfs i.e., 4 and 3 m/min, to achieve the minimum wfs. Table 4 below shows the value of the wfs of the individual wires and the calculated height of each layer by averaging it per layer with the previous layer of the same composition to reduce the error.

Table 4 Layer by Layer wfs of the incremental gradient

No. of Layer	wfs (SS316L) m/min	wfs (IN625) m/min	Average thickness(mm)
1-2	4.0	0	2.0
3-4	3.6	0.4	1.6
5-6	3.2	0.8	1.7
7-8	2.8	1.2	1.3
9-10	2.4	1.6	1.0
11-12	2.0	2.0	1.4
13-14	.6	2.4	1.5
15-16	1.2	2.8	0.9
17-18	0.8	3.2	1.4
19-20	0.4	3.6	1.30
21-22	0	4.0	1.5

In the incremental gradient of total wfs 4.0 m/min, the final total height of the deposited sample is 31.0 mm, while the experimental height of the FGM is 31.2 mm (from Table 4).

In a similar way, the second incremental gradient structure of FGM is fabricated by keeping the total wfs 3.0 m/min.

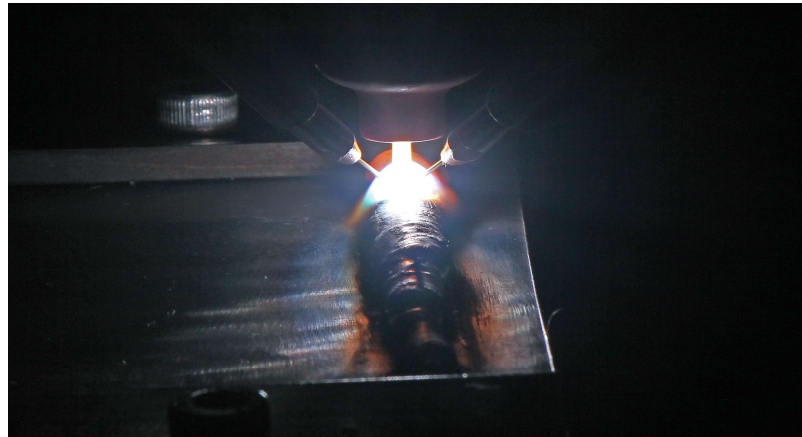


Figure 4.2 Front feeding of the wires during deposition

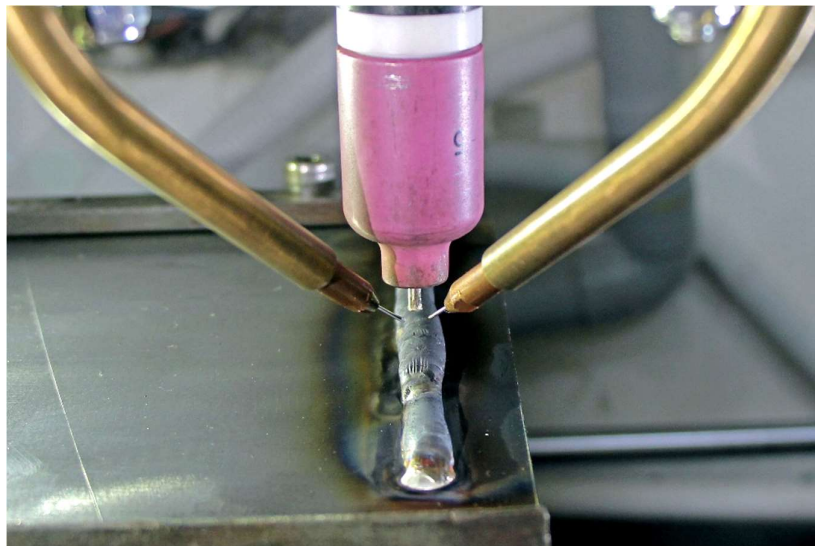


Figure 4.3 Alignment of the wires with the electrode

The material of the substrate used in this research work is AISI 1020; from the previous literature and with the observation in the stereomicroscope the dilution at the interface of the AISI 1020 and deposited SS316L is without any cracks and pores that can be observe in Figure 4.4.

After checking all the parameters and the environmental condition with shielding gas, i.e., Argon (Ar) having a gas flow rate of 10 liters per min during the deposition with WAAM-TIG and keeping the cooling time 4 mins between each layer.

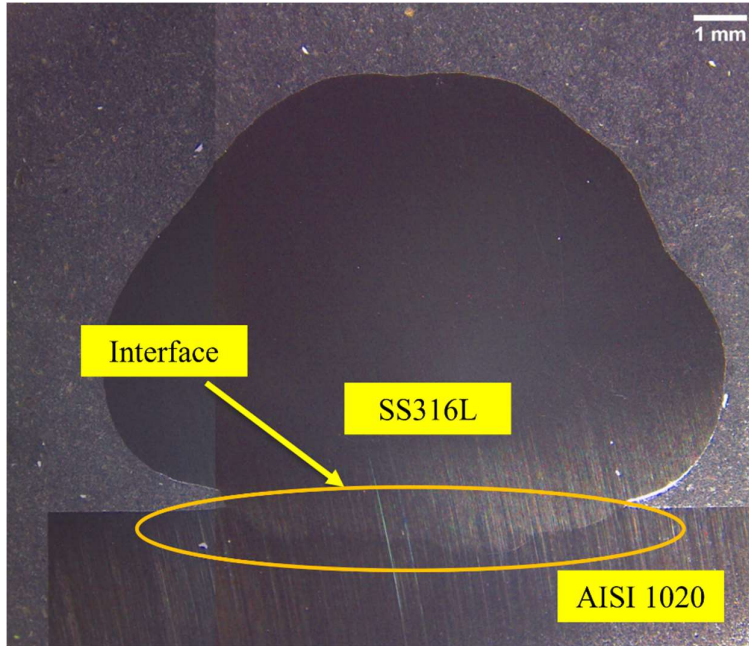


Figure 4.4 Stereoscopic view of the interface of AISI 1020 and SS316L
The final deposition of the incremental gradient structure of FGM is shown in Figure 4.5 when the total wfs is 4.0 m/min. Furthermore, in Figure 4.6 the total wfs is 3.0 m/min. The sample's length is 70 mm.



Figure 4.5 Incremental Gradient Structure wfs 4.0 m/min FGM of SS316L and IN625

In the second incremental gradient of total wfs 3.0 m/min, the final total height of the deposited sample is 26.0 mm, while the experimental height of the FGM is 26.6 mm. The height of the second incremental gradient is less than the first is due to the less quantity of the volume flowing into the arc deposition region. The width of the deposited part for total wfs 4.0 m/min and 3.0 m/min is 8.9 mm and 8.2 mm, respectively.



Figure 4.6 Incremental Gradient Structure wfs 3.0 m/min FGM of SS316L and IN625

During the deposition, due to oxidation of the surface after a few layers, we must wipe out the oxide formation in the nearby region so that it will not total wfs affect the compositional variation in the fabricated FGM. In the primary observation of the deposited FGM, there are no cracks on the surface of each layer in the whole part.

4.3 Sandwich Gradient Structure

The second design opted for this research work is a sandwich-like gradient structure where the SS316L will be 100% at the bottom, and after every 2 layer and a single layer of SS316L, 100% IN625 will be deposited over these layers as per the design. Double layer deposition is named AABB type, while the single-layer deposition is named ABAB type. A represents the 100% SS316L, and B represents the 100% IN625. It can be visualised in Figure 4.7 and Figure 4.8 To maintain the composition of both the materials so that they will be deposited in a controlled manner. In this case, we went with the value of total wfs i.e.,

3 m/min The number of layers in the AABB sandwich structure is 12, while in the ABAB sandwich structure, it is ten layers.

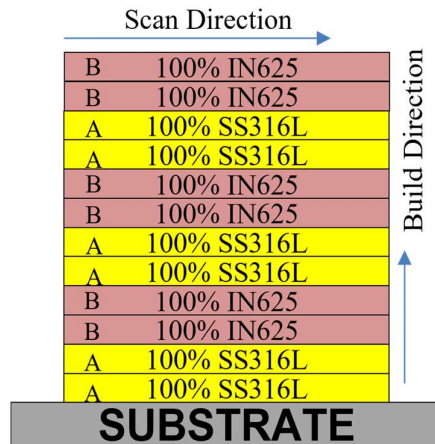


Figure 4.7 Schematic of AABB type gradient structure

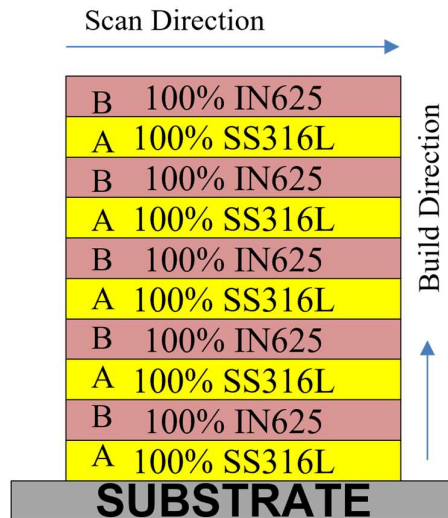


Figure 4.8 Schematic of ABAB type gradient structure

After having a slightly sideways deposition on the upper layer of the incremental gradient structure to overcome this movement the alignment of wires with the electrode change to peripheral alignment is shown in Figure 4.9.

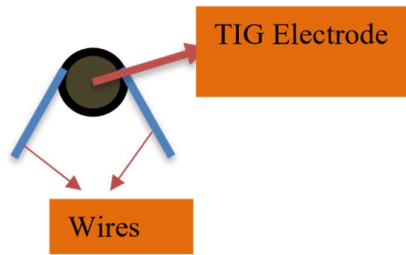


Figure 4.9 Schematic of peripheral alignment of wires

Due to change in alignment, the deposition of layers is observed to be straight in a line as well in Figure 4.10 and Figure 4.11



Figure 4.10 Sandwich AABB gradient structure of FGM

In the sandwich AABB gradient structure, the final total height of the deposited sample is 14.0 mm, while in the sandwich ABAB gradient structure, the final height of the FGM is 11.5 mm. The height of the second incremental gradient is less than the first is due to the less quantity of the volume is flowing into the arc deposition region. The width of the deposited part for AABB and ABAB is 8.0 mm and 7.6 mm, respectively.



Figure 4.11 Sandwich ABAB gradient structure of FGM

In the primarily observation of the deposited FGM, there are no cracks on the surface of each in then the whole part.

4.4 Research Methodology and Sample Preparation

For the EDS, micro-hardness, and microstructure analysis of the FGM, the samples are cut to get the cross-sectional view in the wire-EDM of thickness of 2 mm. Then the samples are hot mounted, and larger samples are cold mounted (Figure 4.12 (a)) with the epoxy to prepare for the analysis through standard metallography techniques, which involves the polishing of the sample through the SiC polishing paper starting from 320 and increasing stepwise as suggested by ASTM ER-11 (2017) till 2500 with continuous monitoring of the samples. Then final polishing for the mirror-like surface finish, diamond polishing of the samples is done with particle size 1.0 μm on the velvet cloth.

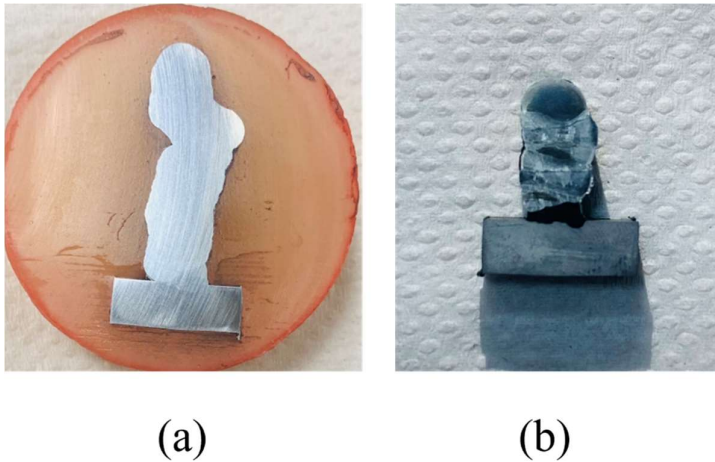


Figure 4.12 (a) Incremental gradient cold mounted sample (b) Sandwich gradient AABB etched sample

The samples were etched electrolytically with 10% oxalic acid with distilled water solution for 10s at 6V. The setup for electrolytically etching is shown in Figure 4.13. After performing the electrolytic etching on the cross-section of the samples, they were analysed using DEWINTER'S digital optical microscope and JEOL 7610F Plus scanning electron microscope (SEM) which is equipped with Oxford

Energy Dispersive Spectrometer (EDS). The microstructure of the FGMs was visible under the optical microscope, and the change in the

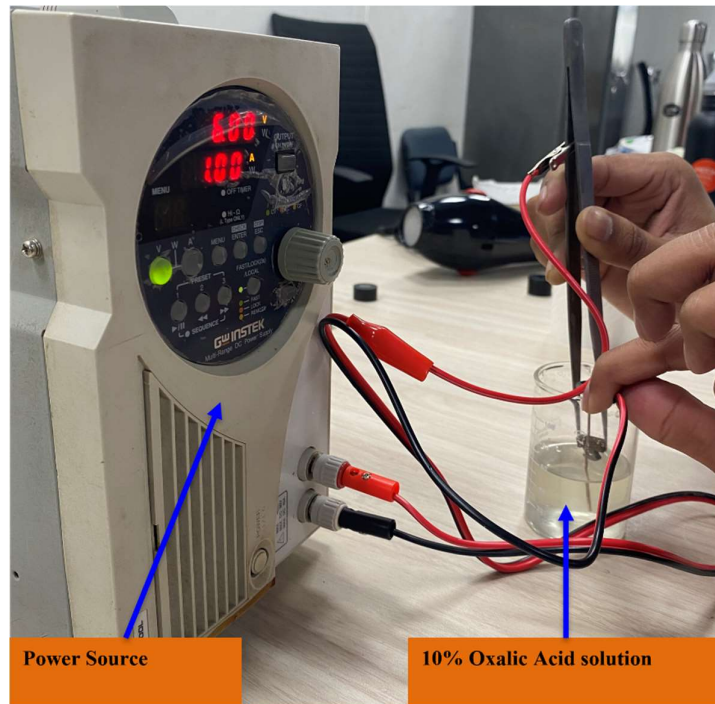


Figure 4.13 Electrolytic etching setup

microstructure corresponded to the content of the composition of Fe, Cr, Ni, and Mo, which can be done by the analysis of elemental composition on the micrograph which was conducted by line scan or EDS mapping. For the FGM samples' mechanical properties, Micro-hardness measurements have been conducted on the samples using the Mitutoyo HM 210A Vickers hardness tester. The samples with polished mirror surfaces were used for micro-hardness testing in which a load of 3N is applied with a total time distributed as 4-10-4 where the first 4 s is for loading, then the following 10 s is for holding; after that, 4 s is for unloading the load. The same load is applied for all the indentations along the building direction, i.e., longitudinal. The gap of 1 mm is kept between the two indentations is constant to avoid any interference. Three indentations were performed at each point across the same height at 1 mm, and the average values were recorded.

Chapter 5

Results and Discussion

5.1 Overview

The design of the FGMs and its fabrication on the experimental setup is performed in the earlier chapters. This chapter will use the research methodology to analyse the two different types of FGMs i.e, Incremental gradient structure and Sandwich gradient structure quantitative analysis, optical micrograph, and the mechanical properties.

5.2 Incremental Gradient Structure

In this section, the results of various material characterisation methods like EDS, which can perform in three ways (i) Line scan, (ii) Area scan, (iii) Point scan, and (iv) Elemental mapping we have performed line scan from bottom of the sample to the top of the sample to analyse the composition of the main elements (Fe, Cr & Ni) throughout the building direction of deposited FGMs incremental gradient structure in this section.

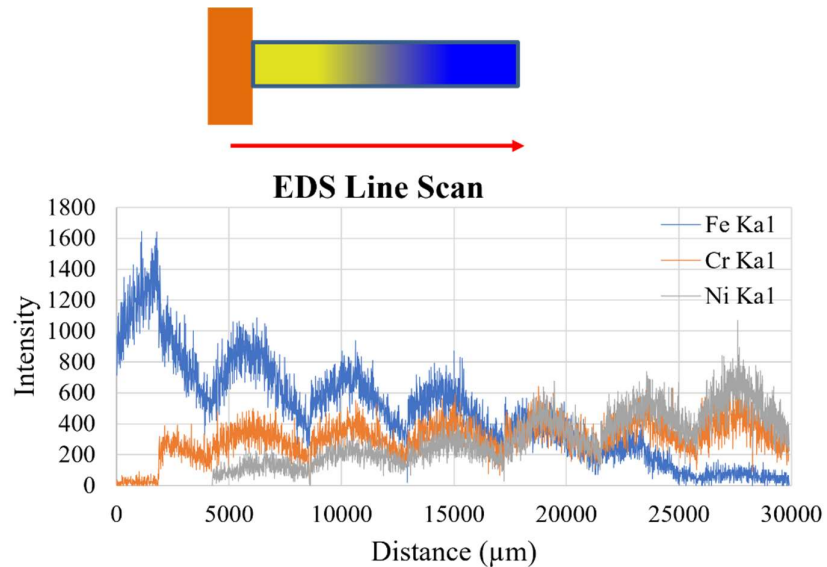


Figure 5.1 EDS line scan of Incremental gradient FGM from bottom to top

The optical images of the vital section have also been captured further the micro-hardness measurements through Vickers hardness testing are done in the building direction.

The EDS line scan graph of both incremental gradient FGM structures shows the same pattern. We plotted the main elements Fe, Ni and Cr intensity values w.r.t distance (μm); the distance is taken from below the interface of the SS316L and AISI 1020 to top of the sample can be seen in Figure 5.1. Elemental mapping of the interface is also analysed to see the substrate's dilution and SS316L.

In Figure 5.1 we can observe up to the 5 mm, the Fe content in the sample is decreasing drastically, which co-relate with Fe content in AISI 1020 is around 99.2% by wt. and in SS316L it is around 65.54% by wt. and as the layer will keep adding the Fe content will go down more, and Ni content which is a major element in IN625 will increase in the incremental gradient FGM sample.

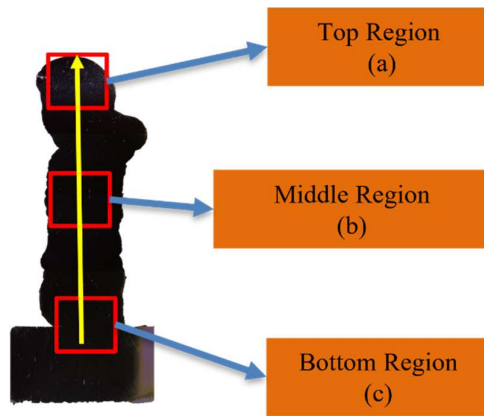
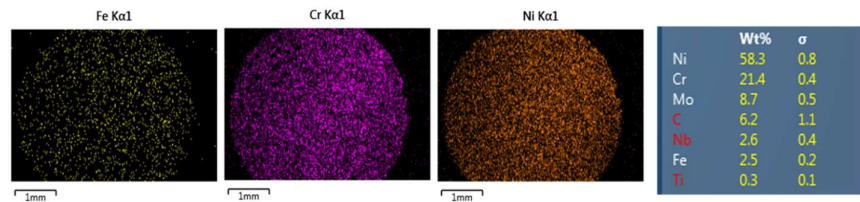


Figure 5.2 EDS line scan region wise for elemental mapping

After the EDS line scan, the elemental mapping is taken at the three regions, top, middle (around 50% SS316L-50% IN625), and bottom region, and the regions are marked in Figure 5.2. A few observations are made from the analysis of the elemental mapping and wt% of the elements in a particular region: -

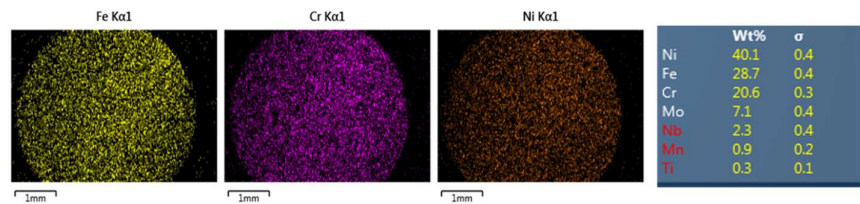
- In Figure 5.5, the elemental mapping of Fe shows most of the region is of the substrate, and the rest is of SS316L, while the

same can be observed from Cr and Ni. The wt% of the region clarifying the same.



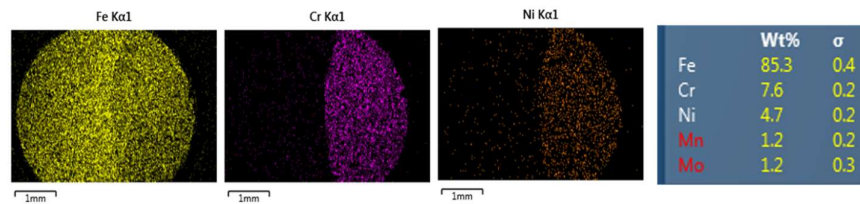
(a)

Figure 5.3 Top Region of incremental gradient FGM elemental mapping



(b)

Figure 5.4 Middle Region of incremental gradient FGM elemental mapping



(c)

Figure 5.5 Bottom Region of incremental gradient FGM elemental mapping

- In middle region (Figure 5.4), the Ni content is more dominating than Fe which can be from the region of 60%IN625 - 40%SS316L.
- As the top region will be complete of IN625, we can also observe with the wt.% data from Figure 5.3 where the Fe content is 2.5%, and the Ni content is around 58%.

- With the quantitative analysis (EDS) and its line scan, the elemental analysis of Incremental gradient FGM structure correlates the designed structure of the FGM.

Electrolytic etching with 10% oxalic acid in DI water solution for 10 s at 6V is done to see the microstructure of the deposited samples from the optical microscope and capture the images of the microstructure from the various region. From literature and previous research, the region to look out for is when the Inconel 625 dominates in the deposition. Despite its unusual appearance, the interface is free of flaws like as cracking, absence of fusion, and delamination.

In this work, the optical images are taken from the region at 50%SS316L - 50%IN625, 40%SS316L – 60%IN625, and 30%SS316L – 70%IN625 composition is present.

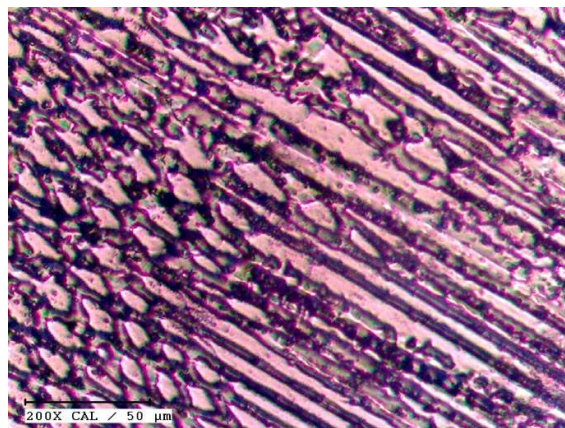


Figure 5.6 Optical image of the region 50%SS316L - 50%IN625

The microstructure of SS316L is predominantly cellular, which is a typical structure for SS316L that has been wire arc additively formed. IN625 has a microstructure that is predominantly columnar dendrites with some equiaxed cellular structure. Columnar dendrites are said to grow in the direction of the arc [36].

In Figure 5.6, the cellular grains are seen, and in half of the region, some equiaxed cellular and mainly columnar dendrites are visible, which suggests the image is taken at the interface or dilution of two materials.

A few observations are made from the analysis of the optical images in the specific region: -

- During consecutive layer deposition, the nucleation and growth of equiaxed dendrites limit the growth of columnar dendrites and hence help the creation of equiaxed dendrites, resulting in the transition of columnar to equiaxed grains. This effect has been frequently seen while using additive manufacturing techniques to fabricate various materials [35].

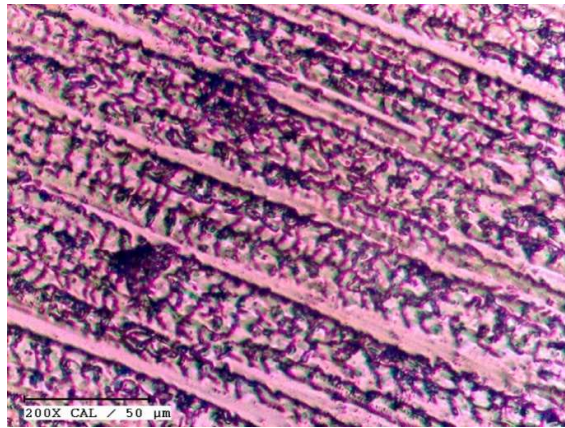


Figure 5.7 Optical image of the region 40%SS316L - 60%IN625

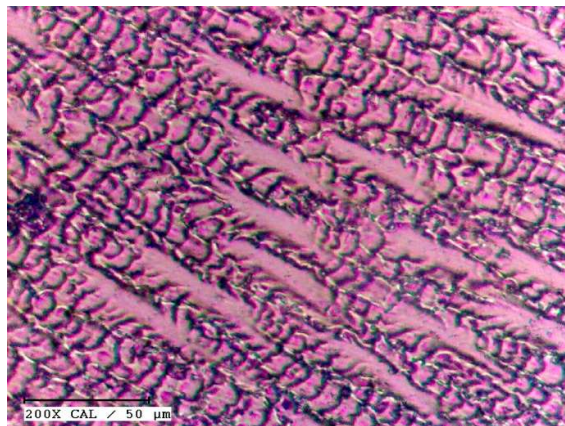


Figure 5.8 Optical image of the region 30%SS316L - 70%IN625

- The columnar dendrites developed slender with narrow primary dendrite arm spacing and short secondary dendrites when the

deposited layer was composed of 40%316L - 60%IN625(Figure 5.7). Furthermore, the presence of equiaxed grains among columnar dendrites showed a reduction in the liquid phase temperature difference in the deposited layer.

- Columnar grains formed due to partial re-melting of the previously deposited layer, allowing previous grains to act as nucleation sites for the current layer's solidification. The latter cladding layer would re-melt the equiaxed structural area on the surface of the earlier cladding layer during the deposition process [30].
- In Figure 5.8, no crack was observed as it was a significant concern during the literature work.

Microhardness of the incremental gradient FGM structure is measured on Mitutoyo HM 210A Vickers hardness (HV) testing machine along the build direction from near to interface to the top of the sample. The indents are taken at 3N load, and the dwell time is 10 s. To minimize the error, the indents are taken 1 mm across the same height and then averaged at 1 mm along the build direction.

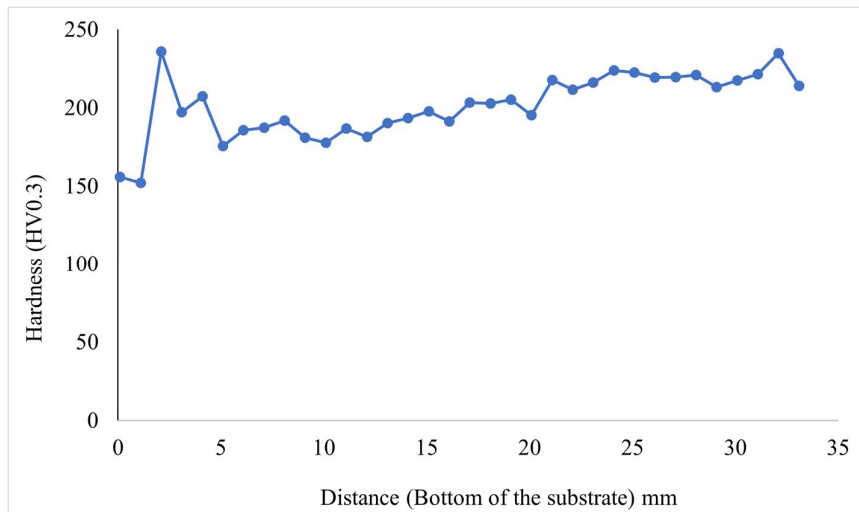


Figure 5.9 Microhardness of Incremental gradient FGM of total wfs 3.0 m/min.

In Figure 5.9 till 3 mm the substrate, interface, and initial layer of SS316L is covered. Due to multiple reheating of the substrate or the

migration of Cr in the interface region, the hardness suddenly spikes. After 3 mm, the hardness value gradually increases according to the design and deposited sample of FGM and ends with a value around 230 HV. The hardness value of IN625 is around the same range. The same data points are observed for the incremental gradient FGM structure with a total wfs 4.0 m/min (Figure 5.10).

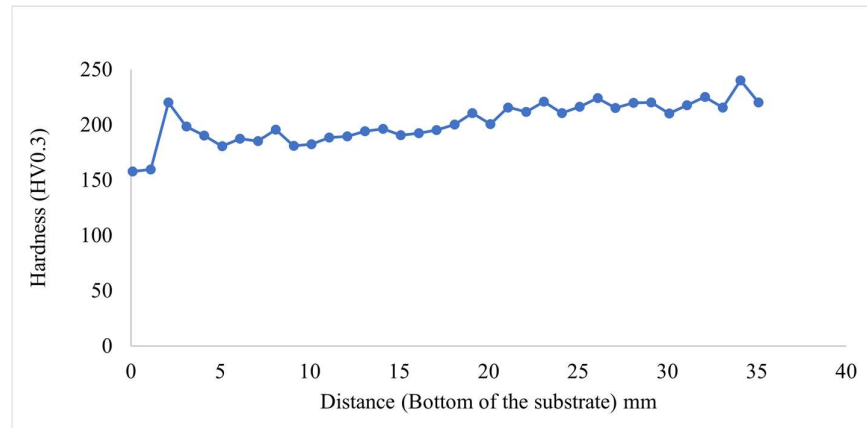


Figure 5.10 Microhardness of Incremental gradient FGM of total wfs 4.0 m/min.

5.3 Sandwich Gradient Structure

In this section, the results of various material characterisation methods like EDS, which can perform in three ways (i) Line scan, (ii) Area scan, (iii) Point scan, and (iv) Elemental mapping we have performed line scan from bottom of the sample to the top of the sample to analyse the composition of the main elements (Fe, Cr & Ni) throughout the building direction of deposited FGMs sandwich gradient structure in this section. The optical images of the important section like the interface have also been captured further the micro-hardness measurements through Vickers hardness testing is done in the building direction. The EDS line scan graph of both sandwich gradient FGM structure AABB and ABAB shows the same pattern, but in AABB type, we can say the due to the 2 layers of pure material diffusion with other material can be observed, while in ABAB type, when we see at top layers it all mixed up somewhat

alloying of the materials looks. We plotted the main elements Fe, Ni, and Cr

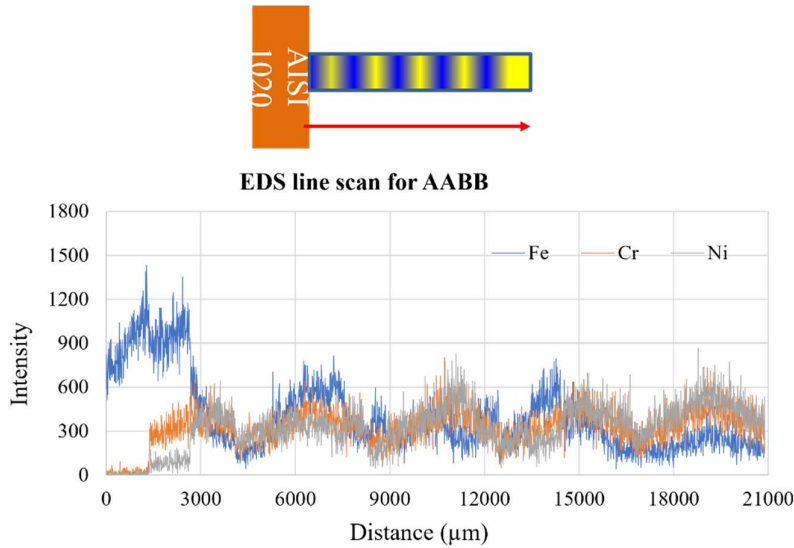


Figure 5.11 EDS line scan of Sandwich gradient ABB FGM from bottom to top

intensity values w.r.t distance (μm). The distance below interface of the SS316L and AISI 1020 to the top of the sample where IN625 is present can be seen in Figure 5.11. Elemental mapping of the interface is also analysed to see the substrate's dilution and SS316L.

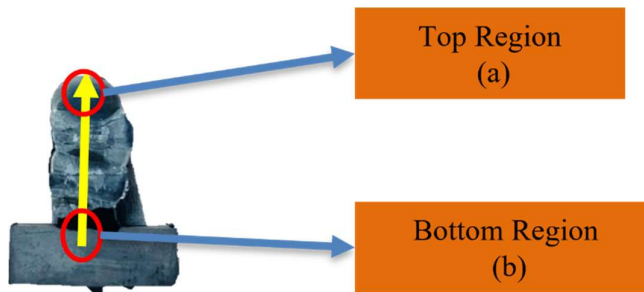
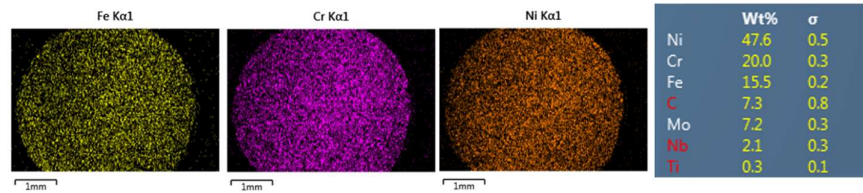


Figure 5.12 EDS line scan region wise for elemental mapping in ABB

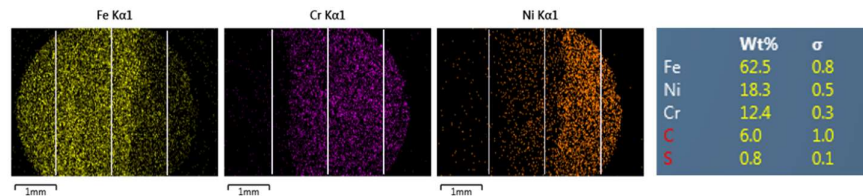
From the EDS line scan of ABB type elements which are into consideration are in increasing gradually and then decreasing gradually. This is going on for Fe and Ni while there is not much variation in Cr.

Thus, the purpose of making the AABB type structure is confirmed with quantitative analyses. Figure 5.12 the marked region, elemental mapping is performed to check the dilution between the substrate and SS316L and, between SS316L and IN625.



(a)

Figure 5.13 Top Region of sandwich AABB gradient FGM elemental mapping



(b)

Figure 5.14 Bottom Region of sandwich AABB gradient FGM elemental mapping

A few observations is made from the analysis of the elemental mapping and wt% of the elements in that particular region for both AABB and ABAB sandwich gradient FGM structure: -

- In Figure 5.14, the mapping is divided into four parts by white line, and it enhances our understanding that it consists of a substrate which at most right then interface after that the dilution layer of SS316L-IN625 as Ni is present in the rightest portion.
- The wt% in Figure 5.13, the Fe content is around 15% due to the alloying at the top surface.

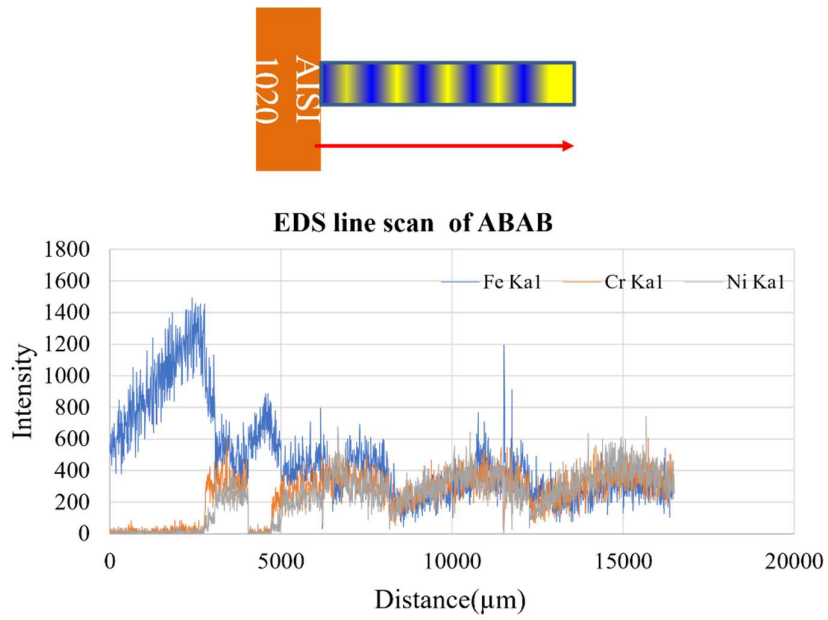


Figure 5.15 EDS line scan of Sandwich gradient ABAB FGM from bottom to top

- The line scan in Figure 5.15 shows the same pattern as the earlier line scans, and as the layers increase, the dilution between the layer dominates and hence the alloying may happen at the top surface. Figure 5.17 gives further confirmation by wt%.

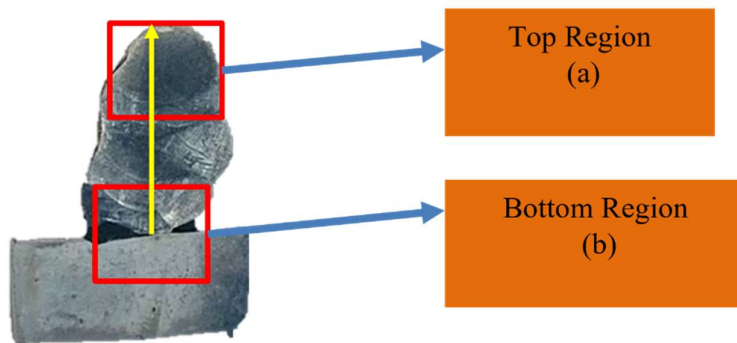
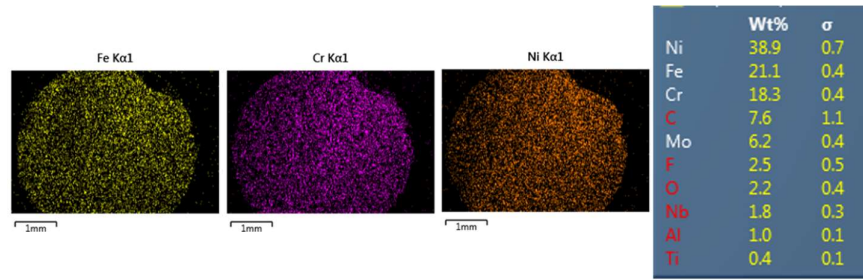
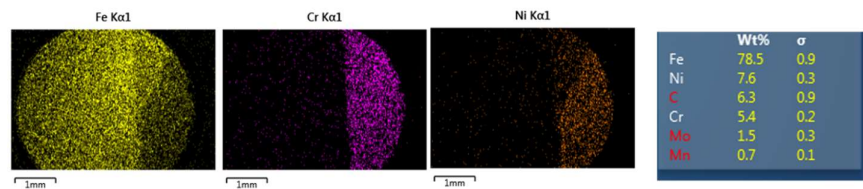


Figure 5.16 EDS line scan region wise for elemental mapping in ABAB



(a)

Figure 5.17 Top Region of sandwich ABAB gradient FGM elemental mapping



(b)

Figure 5.18 Bottom Region of sandwich ABAB gradient FGM elemental mapping

- Since the alloying was suggested from the EDS, this can further give the same observation in the optical image of the top surface of the ABAB type sample. The microstructure with presence of columnar dendrites and the cellular grains which is generally of SS316L when deposit via WAAM-TIG.

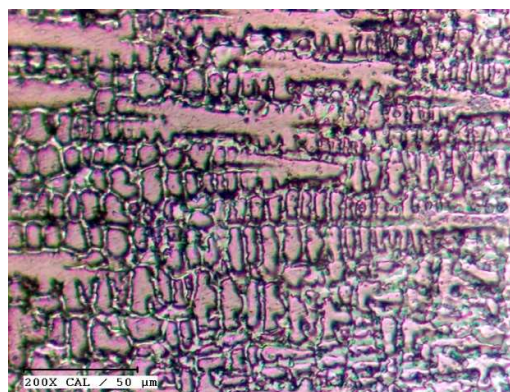


Figure 5.19 Optical Image at the top layer of ABAB structure

- Columnar grains formed as a result of partial re-melting of the previously deposited layer, allowing previous grains to act as nucleation sites for the current layer's solidification.
- In Figure 5.20, the interface between the layers of SS316L-IN625 is visible and suggests alloying at the top region.

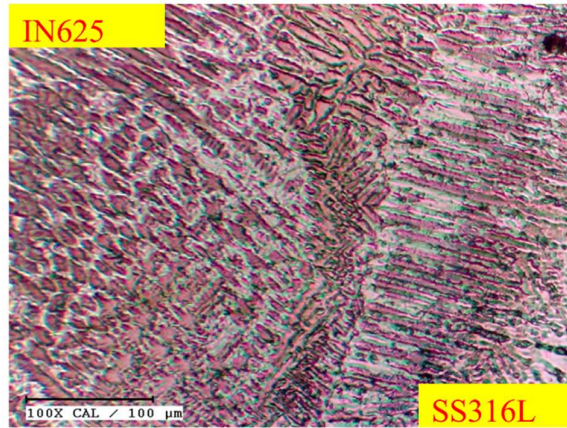


Figure 5.20 Optical Image between the layers at top in ABAB

Microhardness of the incremental gradient FGM structure is measured on Mitutoyo HM 210A Vickers hardness (HV) testing machine along the build direction from near to interface to the top of the sample. The indents are taken at 3N load, and the dwell time is 10 s. The indents are taken 1 mm across the same height and then averaged at 1 mm along the build direction to minimize the error.

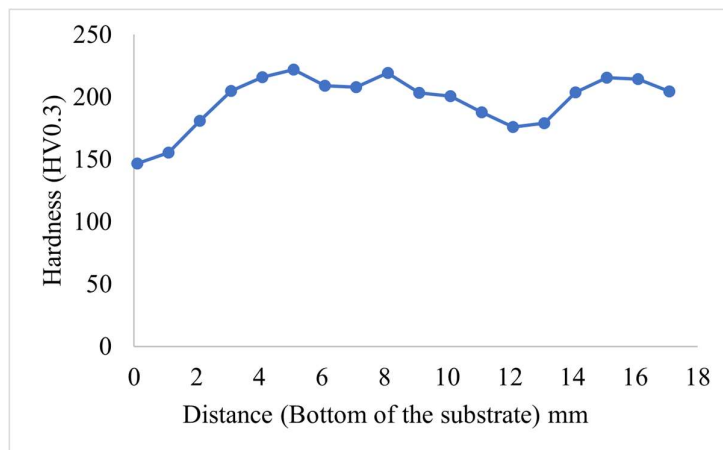


Figure 5.21 Microhardness variation along the height of AABBB FGM

In Figure 5.21, the hardness variation forms a wave pattern which was expected as per the design and content of the AABB type FGM. Around the 6-8 mm, the variation is not in the waveform might be due to the alloying is happening.

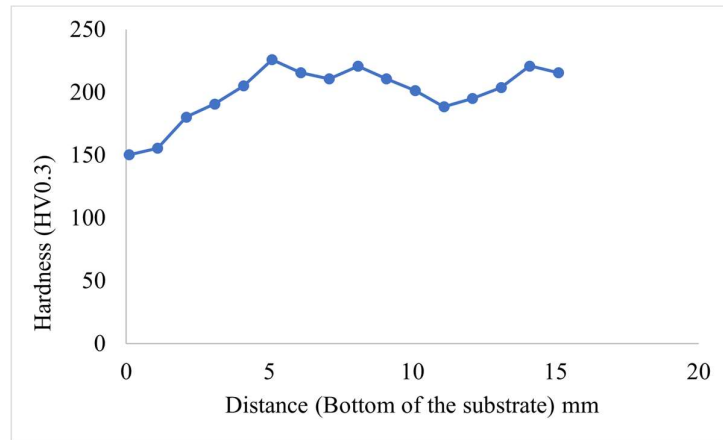


Figure 5.22 Microhardness variation along with the height of ABAB FGM

The hardness variation is more of an abrupt change in this type of FGM due to the compositional changes in every layer. The highest hardness noted in this FGM is around 230 HV.

Chapter 6

Conclusions and Future Scope

6.1 Overview

This chapter concludes with work on the fabrication of Functionally Graded Materials (FGMs) with the WAAM-TIG process, its experimentation, optimisation of the WAAM-TIG process parameters, fabrication, and quantitative analysis microstructure analysis, and mechanical property like microhardness. Further, the future aspects of the research work are discussed.

6.2 Conclusion

The objective of the present study was to fabricate the defect-free FGMs of SS316L-IN625 with various designs to check the feasibility of the process; the deposition is made with the process WAAM-TIG. To check the samples under different tests to find out the properties of the deposited parts.

- Successfully demonstrated the fabrication of different types of FGMs as per the design on the experimental setup with the DED AM method in which the WAAM-TIG process is used.
- The parts fabricated are free from any cracks, pores, and other defects.
- Process parameters are optimised to achieve minimum wfs, i.e., 0.3 m/min.
- The optimised process parameters also have the limit for the maximum wfs, i.e., 4.0 m/min.
- The high wfs wire penetrates the arc region while the low wfs (~0.2m/min) wire cannot enter the arc region, and thus, the deposition is not proper.
- The EDS line scan and elemental mapping analysis confirmed the fabricated samples of both FGMs, i.e., incremental gradient structure and sandwich gradient structure, and the change in the elements over the region or layer.

- There was no fracture observed in the optical microscope and Scanning electron microscope.
- The grain growth is in the wire deposition direction, and that can be observed in microstructures. No cracks were observed in the top region of the incremental gradient FGM.
- The hardness of the fabricated FGMs increases gradually in incremental FGMs and forms a wave pattern in sandwich-like FGMs.

6.3 Future scope

In this section the discussion is about how to take this research work forward and what we can do to enhance the properties of FGMs by varying the process parameters. To investigate the effect of different parameters and compositions, a design of experiments was initiated. Apart from this, the research work can help conduct the corrosion resistance test.

The approach used for this design of experiment is central composite design (CCD).

- This method is used for the response surface methodology to build a second-order, i.e., a quadratic model for the response variable, without needing a full 3^k factorial experiments.
- In this approach, we need 3 levels of continuous variables, consisting of axial points and center points.
- Axial points are required to estimate the quadratic effects, while center points are taken to check for lack of fit or adequacy of fit.
- Three process parameters varied Current, Travel Speed & Concentration.
- The following properties of the deposited bead can be evaluated: bead height & width, composition analysis by EDS, microhardness, and fracture toughness
- The total composition is kept constant for the work i.e., wfs 4.0 m/min. We can vary it in three different ways as 1:3, 3:1, and 2:2. Similarly, the travel speed is taken at 100, 150, and 200 mm/min. Arc current takes the values 170, 212, and 254 A.
- The number of runs in the CCD approach for the current parameters will be 16, but one experiment will be repeated in Table 5.

Table 5 Design of experiment CCD approach parameters

S.No	Composition (SS316-IN625)	Current (A)	Travel Speed (mm/min)
1	3:1	170	100
2		254	
3		170	200
4		254	
5		212	150
6	1:3	170	100
7		254	
8		170	200
9		254	
10		212	150
11	2:2	170	150
12		254	
13		212	100
14		212	150
15		212	200

The above table will provide the base of the experiments to perform and analyse the properties at different parameters.

References

- [1] M. Koizumi, “FGM activities in Japan,” *Composites Part B: Engineering*, vol. 28, no. 1–2, pp. 1–4, Jan. 1997, doi: 10.1016/S1359-8368(96)00016-9.
- [2] A. Kawasaki and R. Watanabe, “Thermal fracture behavior of metal/ceramic functionally graded materials,” *Engineering Fracture Mechanics*, vol. 69, no. 14–16, pp. 1713–1728, Sep. 2002, doi: 10.1016/S0013-7944(02)00054-1.
- [3] R. M. Mahamood and E. T. Akinlabi, “Types of Functionally Graded Materials and Their Areas of Application,” *Topics in Mining, Metallurgy and Materials Engineering*, pp. 9–21, 2017, doi: 10.1007/978-3-319-53756-6_2.
- [4] A. Gupta and M. Talha, “Recent development in modeling and analysis of functionally graded materials and structures,” *Progress in Aerospace Sciences*, vol. 79, pp. 1–14, Nov. 2015, doi: 10.1016/J.PAEROSCI.2015.07.001.
- [5] Z. Liu, M. A. Meyers, Z. Zhang, and R. O. Ritchie, “Functional gradients and heterogeneities in biological materials: Design principles, functions, and bioinspired applications,” *Progress in Materials Science*, vol. 88, pp. 467–498, Jul. 2017, doi: 10.1016/J.PMATSCI.2017.04.013.
- [6] G. H. Loh, E. Pei, D. Harrison, and M. D. Monzón, “An overview of functionally graded additive manufacturing,” *Additive Manufacturing*, vol. 23, pp. 34–44, Oct. 2018, doi: 10.1016/J.ADDMA.2018.06.023.
- [7] R. Mahamood, E. Akinlabi, M. Shukla, and S. L. Pityana, “Functionally Graded Material: An overview,” *Proceedings of the World Congress on Engineering*, Jul. 04, 2012.
- [8] M. Naebe and K. Shirvanimoghaddam, “Functionally graded materials: A review of fabrication and properties,” *Applied Materials Today*, vol. 5, pp. 223–245, Dec. 2016, doi: 10.1016/J.APMT.2016.10.001.
- [9] J. F. Groves and H. N. G. Wadley, “Functionally graded materials synthesis via low vacuum directed vapor deposition,” *Composites Part B: Engineering*, vol. 28, no. 1–2, pp. 57–69, Jan. 1997, doi: 10.1016/S1359-8368(96)00023-6.
- [10] M. Kawase, T. Tago, M. Kurosawa, H. Utsumi, and K. Hashimoto, “Chemical vapor infiltration and deposition to produce a silicon carbide–carbon functionally gradient material,” *Chemical Engineering Science*, vol. 54, no. 15–16, pp. 3327–3334, Jul. 1999, doi: 10.1016/S0009-2509(98)00391-1.

- [11] K. A. Khor and Y. W. Gu, "Effects of residual stress on the performance of plasma sprayed functionally graded ZrO₂/NiCoCrAlY coatings," *Materials Science and Engineering: A*, vol. 277, no. 1–2, pp. 64–76, Jan. 2000, doi: 10.1016/S0921-5093(99)00565-1.
- [12] S. Stewart, R. Ahmed, and T. Itsukaichi, "Contact fatigue failure evaluation of post-treated WC–NiCrBSi functionally graded thermal spray coatings," *Wear*, vol. 257, no. 9–10, pp. 962–983, Nov. 2004, doi: 10.1016/J.WEAR.2004.05.008.
- [13] B. Kieback, A. Neubrand, and H. Riedel, "Processing techniques for functionally graded materials," *Materials Science and Engineering: A*, vol. 362, no. 1–2, pp. 81–106, Dec. 2003, doi: 10.1016/S0921-5093(03)00578-1.
- [14] A. G. Arsha, E. Jayakumar, T. P. D. Rajan, V. Antony, and B. C. Pai, "Design and fabrication of functionally graded in-situ aluminium composites for automotive pistons," *Materials & Design*, vol. 88, pp. 1201–1209, Dec. 2015, doi: 10.1016/J.MATDES.2015.09.099.
- [15] B. Kieback, A. Neubrand, and H. Riedel, "Processing techniques for functionally graded materials," *Materials Science and Engineering: A*, vol. 362, no. 1–2, pp. 81–106, Dec. 2003, doi: 10.1016/S0921-5093(03)00578-1.
- [16] B. Zhang, P. Jaiswal, R. Rai, and S. Nelaturi, "Additive Manufacturing of Functionally Graded Material Objects: A Review," *Journal of Computing and Information Science in Engineering*, vol. 18, no. 4, Dec. 2018, doi: 10.1115/1.4039683/369013.
- [17] W. B. James, "Powder Metallurgy Methods and Applications," *Powder Metallurgy*, pp. 9–19, Dec. 2015, doi: 10.31399/ASM.HB.V07.A0006022.
- [18] W. Li, J. Zhang, X. Zhang, and F. Liou, "Effect of optimizing particle size on directed energy deposition of Functionally Graded Material with blown Pre-Mixed Multi-Powder," *Manufacturing Letters*, vol. 13, pp. 39–43, Aug. 2017, doi: 10.1016/J.MFGLET.2017.07.001.
- [19] J. Alcisto *et al.*, "Tensile properties and microstructures of laser-formed Ti-6Al-4V," *Journal of Materials Engineering and Performance*, vol. 20, no. 2, pp. 203–212, Mar. 2011, doi: 10.1007/S11665-010-9670-9/TABLES/2.
- [20] J. Liu, R. Kannan, D. Zhang, T. Liu, P. Nandwana, and A. Devaraj, "Multi-scale characterization of supersolidus liquid phase sintered H13 tool steel manufactured via binder jet additive manufacturing," *Additive Manufacturing*, p. 102834, Apr. 2022, doi: 10.1016/J.ADDMA.2022.102834.

- [21] F. Zhang *et al.*, “The recent development of vat photopolymerization: A review,” *Additive Manufacturing*, vol. 48, p. 102423, Dec. 2021, doi: 10.1016/J.ADDMA.2021.102423.
- [22] X. Zheng *et al.*, “Ultralight, ultrastiff mechanical metamaterials,” *Science (1979)*, vol. 344, no. 6190, pp. 1373–1377, Jun. 2014, doi: 10.1126/SCIENCE.1252291/SUPPL_FILE/ZHENG.SM.PDF.
- [23] M. Leary, “Material extrusion,” *Design for Additive Manufacturing*, pp. 223–268, Jan. 2020, doi: 10.1016/B978-0-12-816721-2.00008-7.
- [24] S. Kumar, “Development of Functionally Graded Materials by Ultrasonic Consolidation,” *CIRP Journal of Manufacturing Science and Technology*, vol. 3, no. 1, pp. 85–87, Jan. 2010, doi: 10.1016/J.CIRPJ.2010.07.006.
- [25] B. J. de Gans, P. C. Duineveld, and U. S. Schubert, “Inkjet Printing of Polymers: State of the Art and Future Developments,” *Advanced Materials*, vol. 16, no. 3, pp. 203–213, Feb. 2004, doi: 10.1002/ADMA.200300385.
- [26] H. Yang *et al.*, “Performance evaluation of ProJet multi-material jetting 3D printer,” <http://dx.doi.org/10.1080/17452759.2016.1242915>, vol. 12, no. 1, pp. 95–103, Jan. 2016, doi: 10.1080/17452759.2016.1242915.
- [27] B. E. Carroll *et al.*, “Functionally graded material of 304L stainless steel and inconel 625 fabricated by directed energy deposition: Characterization and thermodynamic modeling,” *Acta Materialia*, vol. 108, pp. 46–54, Apr. 2016, doi: 10.1016/J.ACTAMAT.2016.02.019.
- [28] W. Meng, W. Zhang, W. Zhang, X. Yin, and B. Cui, “Fabrication of steel-Inconel functionally graded materials by laser melting deposition integrating with laser synchronous preheating,” *Optics & Laser Technology*, vol. 131, p. 106451, Nov. 2020, doi: 10.1016/J.OPTLASTEC.2020.106451.
- [29] B. Chen, Y. Su, Z. Xie, C. Tan, and J. Feng, “Development and characterization of 316L/Inconel625 functionally graded material fabricated by laser direct metal deposition,” *Optics and Laser Technology*, vol. 123, Mar. 2020, doi: 10.1016/J.OPTLASTEC.2019.105916.
- [30] K. Shah, I. ul Haq, A. Khan, S. A. Shah, M. Khan, and A. J. Pinkerton, “Parametric study of development of Inconel-steel functionally graded materials by laser direct metal deposition,” *Materials and Design*, vol. 54, pp. 531–538, 2014, doi: 10.1016/J.MATDES.2013.08.079.
- [31] J. F. Wang, Q. J. Sun, H. Wang, J. P. Liu, and J. C. Feng, “Effect of location on microstructure and mechanical properties of

- additive layer manufactured Inconel 625 using gas tungsten arc welding,” *Materials Science and Engineering A*, vol. 676, pp. 395–405, Oct. 2016, doi: 10.1016/J.MSEA.2016.09.015.
- [32] S. H. Kim *et al.*, “Selective compositional range exclusion via directed energy deposition to produce a defect-free Inconel 718/SS 316L functionally graded material,” *Additive Manufacturing*, vol. 47, p. 102288, Nov. 2021, doi: 10.1016/J.ADDMA.2021.102288.
- [33] D. C. Hofmann *et al.*, “Compositionally graded metals: A new frontier of additive manufacturing”, doi: 10.1557/jmr.2014.208.
- [34] S. Mohan Kumar *et al.*, “Microstructural Features and Mechanical Integrity of Wire Arc Additive Manufactured SS321/Inconel 625 Functionally Gradient Material,” *Journal of Materials Engineering and Performance*, vol. 30, no. 8, pp. 5692–5703, Aug. 2021, doi: 10.1007/S11665-021-05617-3/FIGURES/13.
- [35] X. Zhang, Y. Chen, and F. Liou, “Fabrication of SS316L-IN625 functionally graded materials by powder-fed directed energy deposition,” <https://doi.org/10.1080/13621718.2019.1589086>, vol. 24, no. 5, pp. 504–516, Jul. 2019, doi: 10.1080/13621718.2019.1589086.
- [36] A. Ullah Khan and Y. K. Madhukar, “Effects of Pillar-Based Substrate on the Wire Arc Additive Manufacturing Process,” *International Journal of Precision Engineering and Manufacturing*, vol. 22, pp. 1311–1321, 123AD, doi: 10.1007/s12541-021-00529-7.